Monthly Notices
of the
ROYAL ASTRONOMICAL SOCIETY

MNRAS **461,** 794–815 (2016)
Advance Access publication 2016 June 15

doi:10.1093/mnras/stw1300

The star formation history and accretion-disc fraction among the K-type members of the Scorpius–Centaurus OB association

Mark J. Pecaut[1]★ and Eric E. Mamajek[2]

[1]*Department of Physics, Rockhurst University, 1100 Rockhurst Rd, Kansas City, MO 64110-2508, USA*
[2]*Department of Physics and Astronomy, University of Rochester, Rochester, NY 14627-0171, USA*

Accepted 2016 May 27. Received 2016 May 26; in original form 2015 December 12

ABSTRACT

We present results of a spectroscopic survey for new K- and M-type members of Scorpius–Centaurus (Sco–Cen), the nearest OB Association (∼100–200 pc). Using an X-ray, proper motion and colour–magnitude selected sample, we obtained spectra for 361 stars, for which we report spectral classifications and Li and Hα equivalent widths. We identified 156 new members of Sco–Cen, and recovered 51 previously published members. We have combined these with previously known members to form a sample of 493 solar-mass (∼0.7–1.3 $M_{\odot}$) members of Sco–Cen. We investigated the star formation history of this sample, and re-assessed the ages of the massive main-sequence turn-off and the G-type members in all three subgroups. We performed a census for circumstellar discs in our sample using *WISE* infrared data and find a protoplanetary disc fraction for K-type stars of $4.4^{+1.6}_{-0.9}$ per cent for Upper Centaurus-Lupus and Lower Centaurus-Crux at ∼16 Myr and $9.0^{+4.0}_{-2.2}$ per cent for Upper Scorpius at ∼10 Myr. These data are consistent with a protoplanetary disc e-folding time-scale of ∼4–5 Myr for ∼1 $M_{\odot}$ stars, twice that previously quoted, but consistent with the Bell et al. revised age scale of young clusters. Finally, we construct an age map of Scorpius–Centaurus which clearly reveals substructure consisting of concentrations of younger and older stars. We find evidence for strong age gradients within all three subgroups. None of the subgroups are consistent with being simple, coeval populations which formed in single bursts, but likely represents a multitude of smaller star formation episodes of hundreds to tens of stars each.

Key words: circumstellar matter – stars: pre-main-sequence – open clusters and associations: individual: Scorpius–Centaurus, Sco OB2, Upper Scorpius, Upper Centaurus-Lupus, Lower Centaurus-Crux.

1 INTRODUCTION AND BACKGROUND

Because of their utility for studying star and planet formation and evolution, a great deal of effort has been directed towards identifying and characterizing samples of nearby young stars. These samples have been indispensable for direct imaging of brown dwarf and planetary-mass companions (e.g. Kraus & Ireland 2012), imaging debris discs in scattered light (e.g. Kalas et al. 2015), exploring the star–disc interaction in young stars (e.g. Nguyen et al. 2009), and studying the evolution of gas-rich and dusty debris discs as a function of age (e.g. Mamajek 2009; Chen et al. 2011).

The nearest of these samples are small, diffuse, nearby associations of kinematically related stars, (e.g. the β Pictoris moving group, TW Hya Association; Zuckerman & Song 2004; Torres et al. 2008). These typically have tens of known members, with masses ∼0.02–2 $M_{\odot}$. While these are extremely useful due to their proximity, studies based on these samples may be subject to small number statistics. Fortunately, there exist large collections of young stars, only slightly more distant, in nearby OB associations. OB associations contain members across the mass spectrum, including the hot and massive O- and B-type stars for which they are named, intermediate-mass A/F stars, lower-mass G/K/M stars, and very low-mass free-floating substellar objects. Though the lower mass (<1.5 $M_{\odot}$) stars blend in with the Galactic field population and are therefore much more difficult to identify than the OB stars, they comprise the dominant stellar component of OB associations, typically present in the thousands (Briceño et al. 2007).

Scorpius–Centaurus (Sco–Cen), the nearest OB association, has been the subject of several efforts to identify its lower mass population (e.g. de Zeeuw et al. 1999; Preibisch & Zinnecker 1999; Mamajek, Meyer & Liebert 2002; Rizzuto, Ireland & Robertson 2011; Rizzuto, Ireland & Kraus 2015). Sco–Cen harbors a barely explored population of thousands of low-mass K and M-type stars

*E-mail: Mark.Pecaut@rockhurst.edu

(Preibisch & Mamajek 2008). The association consists of three classic subregions first defined by Blaauw (1946), and later refined by de Zeeuw et al. (1999): Upper Scorpius (US), Upper Centaurus-Lupus (UCL), and Lower Centaurus-Crux (LCC). The subgroups have mean distances of 145 pc, 140 pc, and 118 pc, respectively (de Zeeuw et al. 1999). Though many K/M type members of US have been identified in surveys by Walter et al. (1994), Preibisch et al. (1998), Preibisch & Zinnecker (1999), Preibisch, Guenther & Zinnecker (2001), Preibisch et al. (2002), and Rizzuto et al. (2015), UCL and LCC occupy larger regions of the sky, and have received less attention, with only ∼90 K/M stars identified in both subgroups, mostly in Mamajek et al. (2002), Preibisch & Mamajek (2008), Song, Zuckerman & Bessell (2012), and a few new M-type members discovered by Rodriguez et al. (2011) and Murphy, Lawson & Bento (2015) using *Galaxy Evolution Explorer* (*GALEX*) UV observations. A deep DECam imaging survey of UCL and LCC is underway which is yielding dozens of members down to the deuterium-burning limit (Moolekamp et al., in preparation).

In this study, we identify and characterize a new sample of K/M-type (∼0.7–1.3 $M_{\odot}$) members of Sco–Cen selected through their X-ray emission and proper motions. We describe the results of a low-resolution spectroscopic survey to identify new low-mass K- and M-type members of Sco–Cen. We combine our newly identified members with members discovered by previous surveys to estimate the accretion disc fraction, and probe the star formation history of each subgroup. Finally, we place these results in context with the results from other stellar populations.

2 SAMPLE SELECTION

We aim to find new K- and M- type members of all three subgroups of Sco–Cen. Low-mass pre-main-sequence stars are X-ray luminous, with $\log(L_x/L_{\rm bol}) \simeq -3$, due to their strong magnetic dynamos and coronal X-ray emission (Feigelson & Montmerle 1999). To build our candidate star list, we cross-referenced the PPMX proper-motion catalogue (Röser et al. 2008) with X-ray sources within 40 arcsec in the *ROSAT* Bright Source (Voges et al. 1999) and Faint Source (Voges et al. 2000) catalogues. We restricted our search to the de Zeeuw et al. (1999) boundaries for Sco–Cen and adopted their proper motion limits with an extra 10 mas yr^{-1} to allow for larger proper motion uncertainties and possible kinematic sub-structure. For objects at a distance of ∼140 pc, this extra 10 mas yr^{-1} translates to $\simeq$7 km s^{-1}. For US, UCL, and LCC this gives limits of $\mu < 47$ mas yr^{-1}, 12 mas yr^{-1} $< \mu <$ 55 mas yr^{-1}, and 15 mas yr^{-1} $< \mu <$ 55 mas yr^{-1}, respectively, with $\mu_\alpha < 10$ mas yr^{-1} and $\mu_\delta < 30$ mas yr^{-1} for all three subgroups. We also required that our proper motions were less than 50 per cent uncertain, $\sigma_\mu < 0.5\mu$, to avoid candidates with poorly constrained proper motions. The mean proper motion magnitude varies across the association due to its large extent on the sky and will also vary for stars of different distances, this being the principle behind kinematic parallaxes. The intrinsic $J-K_S$ colour of an unreddened K0V dwarf is 0.48 mag (Pecaut & Mamajek 2013), and we aimed to find low-mass K- or M-type members of Sco–Cen so we further made colour–magnitude cuts and required our candidates to have colour $J-K_S > 0.5$ mag and magnitude $7.0 < J < 11.0$ from the 2MASS Point Source Catalog (Skrutskie et al. 2006). To avoid very large integration times on the SMARTS 1.5 m telescope, we chose $J < 11.0$ mag, which corresponds to $V \sim 12.5$ mag for an unreddened K0V dwarf. Stars brighter than $J \sim 7.0$ mag would have been covered by previous surveys (e.g. Mamajek et al. 2002), so we chose $J > 7.0$ mag. At the time we performed our sample selection, accurate V-band magnitudes were not available for most stars in our parent sample, so we used J-band magnitudes to filter the brighter and fainter ends of our parent sample. We removed candidates located in UCL just below US, in $343 < l < 350$ and $0 < b < 10$ in galactic coordinates. This region overlaps with 'Lower Sco' (Mamajek 2013; Nguyen, Mamajek & Pecaut 2013; Mamajek et al. 2013), and will be discussed in forthcoming papers (Mamajek et al., in preparation; Nguyen et al., in preparation). This left us with 677 candidates, listed in Table 1. Before assembling a list of targets for observation, we searched the literature to record those stars which had been studied in previous surveys from which spectral type, Li or Hα measurements were available in sufficient detail to make a membership determination. We then omitted stars which were studied in Mamajek et al. (2002), Preibisch et al. (1998), Preibisch et al. (2001), Preibisch et al. (2002), Ardila, Martín & Basri (2000), Köhler et al. (2000), Slesnick, Carpenter & Hillenbrand (2006), Krautter et al. (1997), Wichmann et al. (1997), Riaz, Gizis & Harvin (2006), and Torres et al. (2006). This left us with 365 candidates in our spectroscopic target list. Objects PPMX J121431.8-511015, PPMX J134751.4-490148, PPMX J143751.3-545649, and PPMX J154348.8-392737 were not observed because they were within 60 arcsec of known Sco–Cen members. The first two may constitute new companions to Sco–Cen members MML 9 and MML 38, respectively (listed in Table 2). The status of the third (PPMX J143751.3-545649) with respect to MML 47 is unclear. The fourth, PPMX J154348.8-392737, is a previously catalogued companion to HD 140197 (listed as SEE 247 AB in the Washington Double Star catalogue; Mason et al. 2001). This finally leaves 361 candidates which were spectroscopically observed.

3 OBSERVATIONS AND DATA

3.1 Spectra

Low-resolution red (∼5600 Å–6900 Å) optical spectra were obtained from the SMARTS 1.5m telescope at Cerro Tololo Inter-American Observatory (CTIO), Chile. Observations were made in queue mode with the RC spectrograph between 2009 July and 2010 October, and in classical mode during the nights of UT 2010 April 7–17. The spectra were taken with the '47/Ib' setup, which consists of a grating with groove density of 831 grooves mm^{-1}, blaze wavelength 7100 Å, a GG495 filter and a slit width of 110.5μm, giving a spectral resolution of ∼3.1 Å in the red optical. One comparison arc of Ne was taken immediately before three consecutive exposures of each target. The data were reduced using the SMARTS RC Spectrograph IDL pipeline written by Fred Walter.[1] The three object images are median filtered, bias-trimmed, overscan- and bias-subtracted, and flat-fielded. The spectrum is wavelength-calibrated using the Ne comparison frames. Finally, we normalize the spectra to the continuum with a low order spline in preparation for spectral classification.

In addition, we reanalyzed the low resolution spectra from the Mamajek et al. (2002) study. These blue and red spectra were taken at Siding Springs Observatory in UT 2000 April 20–24. The blue spectra have spectral resolution of ∼2.8 Å with spectral coverage of ∼3850–5400 Å. The red spectra have spectral resolution of ∼1.3 Å with spectral coverage of ∼6200–7150 Å. Further details regarding these spectra are described in Mamajek et al. (2002).

[1] http://www.astro.sunysb.edu/fwalter/SMARTS/smarts_15msched.html#RCpipeline

Table 1. Photometry and proper motion data for candidates in the Sco–Cen region.

2MASS	μ_α (mas yr^{-1})	μ_δ (mas yr^{-1})	Ref.	V (mag)	Ref.	B–V (mag)	Ref.	J (mag)	H (mag)	K_S (mag)	Note
10004365-6522155	−11.7 ± 1.9	12.4 ± 1.9	PX	10.972 ± 0.046	A7	0.650 ± 0.077	A7	9.614 ± 0.026	9.193 ± 0.026	9.018 ± 0.019	
10065573-6352086	−19.6 ± 1.5	10.3 ± 1.8	U4	10.950 ± 0.012	A7	0.862 ± 0.018	A7	9.262 ± 0.028	8.744 ± 0.061	8.580 ± 0.024	
10092184-6736381	−14.6 ± 1.8	19.6 ± 1.0	U4	11.512 ± 0.017	A7	0.849 ± 0.051	A7	10.027 ± 0.026	9.497 ± 0.024	9.382 ± 0.021	
10111521-6620282	−26.5 ± 1.6	11.3 ± 1.6	U4	12.242 ± 0.028	A7	0.825 ± 0.035	A7	10.680 ± 0.024	10.223 ± 0.026	10.073 ± 0.023	
10293275-6349156	−11.3 ± 1.4	14.7 ± 1.5	U4	11.373 ± 0.014	A7	0.822 ± 0.027	A7	9.818 ± 0.022	9.349 ± 0.022	9.290 ± 0.019	

Adopted 2MASS JHK_S magnitudes are PSF-fit photometry unless otherwise specified; (a) 2MASS JHK_S aperture photometry; (b) 2MASS JHK_S 6x catalogue (Cutri et al. 2012a); (c) 2MASS H psf photometry / JK_S aperture photometry.
References – (PX) PPMX, Röser et al. (2008); (U4) UCAC4, Zacharias et al. (2013); (T2) Tycho-2, Høg et al. (2000); (A6) APASS DR6 (Henden et al. 2012); (A7) APASS DR7 (Henden et al. 2012); (HP) *Hipparcos*, ESA (1997); (W97) Wichmann et al. (1997); (T06) Torres et al. (2006).
Only the first five rows are shown; this table is available in its entirety in the electronic version of the journal.

3.2 Photometry

Our compiled photometry is listed in Table 1. Six of our candidates have *BV* photometry available from the *Hipparcos* catalogue, and we adopted it where possible. For ∼130 candidates, we adopted *BV* photometry from the Tycho-2 Catalog (Høg et al. 2000), converted to the Johnson system using the conversions in Mamajek et al. (2002), Mamajek, Meyer & Liebert (2006). For ∼350 candidates, we adopted *BV* photometry from the AAVSO Photometric All-Sky Survey[2] (APASS) Data Release 6 and Data Release 7 (Henden et al. 2012). and the Search for Associations Containing Young stars catalogue (SACY; Torres et al. 2006) for ∼100 candidates. For stars with $V \lesssim 12$ mag, conservative estimates for SACY photometric uncertainties are 0.01 mag (C.A.O. Torres, private communication). We adopt JHK_S photometry from the Two Micron All-Sky Survey Point Source Catalog (2MASS; Skrutskie et al. 2006). We adopt 2MASS aperture photometry when the PSF is poorly fit as indicated by the quality flags ('qflg' other than 'A') in the 2MASS catalogue. These data are indicated in the notes of Table 1.

For candidate members, we use mid-IR photometry from the *Wide-field Infrared Survey Explorer* (*WISE*; Wright et al. 2010; Cutri et al. 2012b). We visually examined all images of members which exhibit infrared excesses (identified in Section 4.9.2) in one or more *WISE* bands. We flagged photometry which could be affected by blends with adjacent objects, unresolved binaries, or extended emission from nearby bright stars. We exclude photometry with unreliable detections or uncertainties exceeding 0.25 mag. We followed the scheme for evaluating the photometry in Luhman & Mamajek (2012). Our mid-IR *WISE* photometry is listed in Table 3.

A few stars in our sample had *WISE* photometry contaminated by nearby objects. PDS 415 and CD-23 12840 are a ∼4 arcsec binary, but only CD-23 12840 is in the PPMX catalogue and thus only CD-23 12840 is in our sample. Both components of the pair are listed in the *WISE* All-Sky catalogue but CD-23 12840 has $K_S - W1 < 0.0$. Examination of the *WISE* images shows the two are blended. PDS 415 is detected as an infrared source in the AKARI catalogue (Ishihara et al. 2010) but CD-23 12840 is not detected. Thus we conclude that PDS 415 is the source of the infrared excess and the CD-23 12840 K_S band excess may be spurious. We exclude the CD-23 12840 *WISE* photometry. HD 326277 is blended with a nearby object in *W*1 and *W*2 and had no reliable detection in *W*3 and *W*4. HD 326277 has *Spitzer* 3.6 μm and 4.5 μm IRAC photometry in *GLIMPSE* ([3.6] = 8.165±0.040 mag, [4.5] = 8.178±0.044 mag; Churchwell et al. 2009) which differs from the *WISE* *W*1 and *W*2 by ∼0.5 mag. This suggests that the *WISE* photometry for this star is contaminated by blends and therefore we exclude the *WISE* photometry for HD 326277.

3.3 Astrometry

Although our original selection scheme utilized proper motions from the PPMX catalogue, we adopt proper motions for our analysis from several catalogues, including the *Hipparcos* catalogue (van Leeuwen 2007), the Tycho-2 catalogue (Høg et al. 2000), the PPMX catalogue (Röser et al. 2008) and the UCAC4 catalogue (Zacharias et al. 2013). At the time we performed our sample selection, the PPMX catalogue the most complete homogeneous proper motion catalogue with absolute proper motions (i.e. on the International Celestial Reference System, or ICRS; Röser et al. 2008).

[2] http://www.aavso.org/apass

Table 2. New candidate double stars in Sco–Cen.

Primary name	Primary PPMX	Secondary PPMX	J (mag)	PA (deg)	Sep. (arcsec)	Epoch (yr)	Notes
MML 9	121434.0-511012	121431.8-511015	8.7,10.0	261.34	21.17	2010.5589	1,2
MML 38	134750.5-490205	134751.4-490148	9.3,10.1	27.36	19.01	2010.5589	2

Notes. (1) The RAVE 4th data release (Kordopatis et al. 2013) reports radial velocities of $12.6 \pm 3.5\,\mathrm{km\,s^{-1}}$ and $11.3 \pm 3.6\,\mathrm{km\,s^{-1}}$ for the primary and secondary, respectively, supporting the notion that they constitute a physical pair. (2) Astrometry from AllWISE positions (Cutri et al. 2014).

However, for our analysis we make use of proper motions for kinematic distance estimates, and therefore desire the most precise and well-constrained proper motions available. Therefore, for our calculations, we select the source catalogue on a case-by-case basis, adopting the proper motions which have the smallest uncertainties. The majority of our adopted proper motions listed in Table 1 are from the UCAC4 catalogue.

4 ANALYSIS

4.1 Spectral classification

The optical spectra were visually classified against a dense grid of carefully chosen spectral standards[3] with spectral coverage from ∼5600 Å–6900 Å. We use the same spectral standards and classification criteria as described in Pecaut & Mamajek (2013). The G/K stars are on the classification system of Keenan & McNeil (1989) and the M-type stars are on the classification system of Kirkpatrick, Henry & McCarthy (1991).

While estimating temperature types for our sample we ignored the Na I doublet at ∼5889/5896 Å because it increases in strength with surface gravity, and is thus useful in discriminating between dwarfs and giants. For those pre-main-sequence (pre-MS) members of Sco–Cen, we expected these to have a Na I doublet line similar to but weaker than dwarfs (Spinrad 1962; Lawson, Lyo & Bessell 2009; Schlieder et al. 2012). Once a temperature type had been established, we compared the Na I doublet to that of a dwarf and a giant of the same temperature subclass, assigning an appropriate luminosity class. In a few cases the star had a Na I doublet feature which closely resembled a giant (luminosity class III) but the relative strength of the Ca I at λ 6102, λ6122 and λ6162 lines relative to the Fe I line at λ6137 resembled that of a dwarf (luminosity class V). In these cases we assigned the intermediate luminosity class of a subgiant (luminosity class IV). For the early to mid G-type stars, the Na I doublet for subgiants is nearly indistinguishable from that of dwarfs (see Fig. 2), so the Na I doublet was only used to assign luminosity classes from spectral type ∼G5 to ∼M3.

We also revised the spectral classifications for Sco–Cen members studied in Mamajek et al. (2002). The spectral types from Mamajek et al. (2002) were tied very closely to those of the Michigan Spectral Survey (Houk 1978, 1982). The Mamajek et al. (2002) spectra were re-classified by M. Pecaut during the survey of Pecaut & Mamajek (2013) using the standards of Keenan & McNeil (1989), and systematic differences were noted. In Table 4 we adopt the revised classifications for the Mamajek et al. (2002) stars. There are clearly systematic differences between the Michigan types and those on the modern MK system (as noted in appendix C.1 of Pecaut & Mamajek 2013). Put simply, a G2V star classified in the Michigan survey corresponds more closely to a G0.5V on the modern grid of G-dwarf standards (Keenan & McNeil 1989), as classified by Gray and collaborators (e.g. Gray et al. 2003, 2006). This is verified by comparison of the colours and effective temperatures of stars classified both by Houk and Gray et al. While the Michigan survey mostly relied on the MK system of Johnson & Morgan (1953) (including changes up through early 1970s), there were minor shifts to the MK system for stars hotter than G0 by Morgan (Morgan & Keenan 1973; Morgan, Abt & Tapscott 1978), and for GK-type stars by Keenan & McNeil (1989) after the Michigan survey was initiated in the late 1960's. The modern M dwarf classifications rely on the standard sequence of Kirkpatrick et al. (1991) and its later additions (e.g. Henry et al. 2002). The spectral classification surveys of bright stars undertaken by Gray and collaborators (Gray, Napier & Winkler 2001; Gray et al. 2003, 2006) are based on the last generations of Morgan's and Keenan's hot and cool star spectral sequences (Morgan et al. 1978, Keenan & McNeil 1989) which are in common modern use. We compared stars of given spectral type in the Michigan survey to those of Gray et al. (2001, 2003, 2006), and in Table 5 we provide an estimate of the modern dwarf spectral type for given Michigan spectral types. Very few of the Michigan spectral classes appear to correspond closely to the same type of star on the modern MK grid (e.g. F6V, K0V, K3V being rare exceptions). Unfortunately, the differences are most pronounced in the early G-type dwarfs, where Michigan G2V corresponds to Gray's G0.5V, Michigan G3V corresponds to G1.5V, etc. This is partially due to Houk's choice of G dwarf standards (e.g. using β Com as their G2V standard, despite it being considered a G0V or F9.5V standard elsewhere), but also due to Keenan's minor adjustments to the G dwarf standards throughout the 1980's. As the Keenan & McNeil (1989) grid defines the modern GK dwarf sequence and is common use, classifications that used this grid are to be considered on the modern MK system following Table 5. For intercomparison of samples of stars classified in the Michigan survey with samples classified on the modern MK system, we recommend converting the Michigan spectral types to the modern MK system using the conversions in Table 5. None map exactly to G2V.

4.2 Distance Calculation

Very few of our candidate members have measured trignometric parallaxes, so we estimate distances to each candidate by calculating a 'kinematic' or 'cluster' parallax (e.g. de Bruijne 1999a). This method uses the centroid space motion of the group with the proper motion of the candidate member and the angular separation to the convergent point of the group to estimate the distance to the individual member, with the assumption that they are comoving. We emphasize that kinematic parallaxes are only meaningful for true members and meaningless for non-members. Kinematic parallaxes have been shown to reduce the scatter in the H–R diagram for cluster members over trignometric parallaxes (de Bruijne 1999b).

[3] See http://www.pas.rochester.edu/emamajek/spt/

Table 3. Infrared photometry and infrared excesses for members of Sco–Cen.

2MASS *J*	*WISE J*	*W1* (mag)	*W2* (mag)	*W3* (mag)	*W4* (mag)	$E(K_S - W1)$ (mag)	$E(K_S - W2)$ (mag)	$E(K_S - W3)$ (mag)	$E(K_S - W4)$ (mag)
10065573-6352086	100655.70-635208.6	8.513 ± 0.023	8.531 ± 0.021	8.446 ± 0.018	8.301 ± 0.131	−0.025 ± 0.033	−0.006 ± 0.032	0.041 ± 0.030	0.115 ± 0.133
10092184-6736381	100921.83-673637.9	9.056 ± 0.019	9.177 ± 0.018	9.201 ± 0.020	8.916 ± 0.190	0.233 ± 0.028	0.142 ± 0.028	0.078 ± 0.029	0.291 ± 0.191
10313710-6901587	103137.09-690158.7	9.414 ± 0.023	9.431 ± 0.021	9.360 ± 0.025	9.622 ± 0.435	−0.013 ± 0.034	−0.011 ± 0.033	0.013 ± 0.035	−0.325 ± 0.436
10334180-6413457	103341.79-641345.6	9.236 ± 0.025	9.218 ± 0.021	9.167 ± 0.030	–	−0.038 ± 0.035	−0.001 ± 0.032	0.003 ± 0.038	–
10412300-6940431	104122.96-694042.8	8.304 ± 0.022	8.330 ± 0.020	8.216 ± 0.015	7.858 ± 0.082	−0.008 ± 0.030	0.012 ± 0.028	0.093 ± 0.025	0.382 ± 0.084

All infrared photometry (*W1*, *W2*, *W3* and *W4*) above is adopted from the *WISE* catalogue (Cutri et al. 2012b). Only the first five rows are shown; this table is available in its entirety in the electronic version of the journal.

We adopt the formalism and methods of Mamajek (2005) and adopt the updated Sco–Cen subgroup space motions listed in Chen et al. (2011). In addition to providing improved distance estimates over simply adopting the mean subgroup distances, the kinematic parallaxes allow us identify non-members and assess the likelihood that the candidate member is a bona-fide member.

4.3 Membership criteria

In order to identify likely members from our sample, we demand that all available data paint a consistent picture of association membership, and therefore consider several indicators to discriminate against interlopers. Based on previous surveys (see Preibisch & Mamajek 2008, and references therein), we expect the K and M-type stars to be pre-MS, and therefore have Li absorption stronger, on average, than that of a ∼30–50 Myr-old population. We also expect that they will exhibit surface gravities intermediate between dwarfs and giants. We identify those stars which have the following.

(i) Appropriate levels of Li absorption in their spectra, using the Li 6708 Å line,
(ii) Dwarf or subgiant surface gravities, using the Na I doublet at 5889/5896 Å,
(iii) Kinematic distances consistent with Sco–Cen,
(iv) H–R diagram positions broadly consistent with membership in Sco–Cen (e.g. neither below the main sequence nor above a 1 Myr isochrone).

We discuss these criteria in detail in the following sections. Borderline cases were examined closely.

4.3.1 Lithium

Pre-MS stars transition from fully convective to having deep convective envelopes with radiative interiors during their contraction. These stars can mix Li from the stellar photosphere throughout the convection zone down to interior regions of the star where it is destroyed at $T \gtrsim 2.6$ MK (Bodenheimer 1965; Strom 1994). Thus, for ∼0.7–1.3 $M_\odot$ stars like those targeted in this study, a high photospheric Li abundance is only present when the star is very young. Based on the published ages (de Geus, de Zeeuw & Lub 1989; Preibisch & Zinnecker 1999; Mamajek, Meyer & Liebert 2002; Pecaut, Mamajek & Bubar 2012), we expect members of Sco–Cen to exhibit stronger Li absorption lines at a given $T_{\rm eff}$, on average and within some acceptable scatter, than a ∼30–50 Myr sample.

We measured the equivalent width of the 6708 Å Li feature for all stars in our spectroscopic sample. The values were measured with IRAF[4] with Vogt profiles after the spectrum was normalized to the continuum. Given our spectral resolution and the repeatability of our measurements, we estimate that our reported EW(Li) values are accurate to ∼0.05 Å. The 6708 Å feature is a blend with a nearby Fe I line at 6707.44 Å, unresolved at our resolution, and thus our EW(Li) values are probably overestimated by ∼0.02 Å. However, this is smaller than our uncertainties and we do not attempt to correct for this blend. Many stars in our parent sample were not observed because they had EW(Li) values available in the literature; for these stars we simply adopted the previously published values.

[4] IRAF is distributed by the National Optical Astronomy Observatory, which is operated by the Association of Universities for Research in Astronomy (AURA) under cooperative agreement with the National Science Foundation.

Table 4. Membership properties for Sco–Cen candidates.

2MASS	SpT	Ref.	EW(Li) (Å)	Ref.	Membership Li?	μ?	log (g)?	HRD?	Final	Young Star Ref.	Sco–Cen Ref.
10004365-6522155	G3V	PM	0.24	PM	Y	N	Y?	–	N	–	–
10065573-6352086	K0Ve	T06	0.35	T06	Y	Y	–	Y	Y	T06	PM
10092184-6736381	K1IV(e)	PM	0.32	PM	Y	Y	Y?	Y	Y	PM	PM
10111521-6620282	K0IV	PM	0.33	PM	Y	Y	Y?	N	N	–	–
10293275-6349156	K1IV	PM	0.23	PM	Y?	N	Y?	–	N	–	–

References in the final two columns refer to the first work to identify the star as young ('Young Star Ref.') and the first work to identify it as a member of Sco–Cen ('Sco–Cen Ref.').
References – (PM) – This work; (S49) – Struve & Rudkjøbing (1949); (H54) – Henize (1954); (D59) – Dolidze & Arakelyan (1959); (T62) – The (1962); (T64) – The (1964); (G67) – Garrison (1967); (S72) – Satyvaldiev (1972); (F75) – Filin & Satyvoldiev (1975); (P75) – Petrov & Satyvoldiev (1975); (H76) – Henize (1976); (S77) – Schwartz (1977); (S82) – Satyvoldiev (1982); (S86) – Stephenson (1986); (F87) – Finkenzeller & Basri (1987); (D88) – Downes & Keyes (1988); (He88) – Herbig & Bell (1988); (Ho88) – Houk & Smith-Moore (1988); (I89) – Ichikawa & Nishida (1989); (M89) – Mathieu, Walter & Myers (1989); (S91) – Stocke et al. (1991); (V91) – Vazquez & Feinstein (1991); (B92) – Bouvier & Appenzeller (1992); (C92) – Carballo, Wesselius & Whittet (1992); (G92) – Gregorio-Hetem et al. (1992); (H94) – Hughes et al. (1994); (W94) – Walter et al. (1994); (R95) – Randich et al. (1995); (B96) – Brandner et al. (1996); (P96) – Park & Finley (1996); (F97) – Feigelson & Lawson (1997); (K97) – Krautter et al. (1997); (W97) – Wichmann et al. (1997); (M98) – Martin et al. (1998); (P98) – Preibisch et al. (1998); (S98) – Sciortino et al. (1998); (D99) – de Zeeuw et al. (1999); (P99) – Preibisch & Zinnecker (1999); (W99) – Wichmann et al. (1999); (H00) – Hoogerwerf, de Bruijne & de Zeeuw (2000); (K00) – Köhler et al. (2000); (W00) – Webb (2000); (P01) – Preibisch et al. (2001); (Z01) – Zuckerman et al. (2001); (M02) – Mamajek et al. (2002); (P02) – Preibisch et al. (2002); (R03) – Reid (2003); (M05) – Mamajek (2005); (T06) – Torres et al. (2006); (R06) – Riaz et al. (2006); (Ri06) – Riaud et al. (2006); (C06) – Carpenter et al. (2006); (W07) – White, Gabor & Hillenbrand (2007); (V09) – Viana Almeida et al. (2009); (K11) – Kiss et al. (2011); (R11) – Rodriguez et al. (2011); (L12) – Luhman & Mamajek (2012); (M12) – Mamajek et al. (2012); (S12) – Song et al. (2012); (R15) – Rizzuto et al. (2015); (A) – measured from spectrum downloaded from the ESO archive, programme 083.A-9003(A); (B) – measured from spectrum downloaded from the ESO archive, programme 081.C-0779(A).
Only the first five rows are shown; this table is available in its entirety in the electronic version of the journal.

Table 5. Comparing Michigan spectral types to Gray MK spectral types.

(1) SpT Houk		(2) SpT Gray	(3) SpT Houk		(4) SpT Gray	(5) SpT Houk		(6) SpT Gray
F0V	→	F1V	G0V	→	F9.5V	K0V	→	K0V
F1V	→	F2V	G0/1V	→	F9.5V	K0/1V	→	K1V
F2V	→	F3.5V	G0/2V	→	G3:V	K1V	→	K1.5V
F2/3V	→	F3.5V	G1V	→	G0+V	K1/2V	→	K2V
F3V	→	F4V	G1/2V	→	G0V	K2V	→	K2.5V
F3/5V	→	F5V	G2V	→	G0.5V	K2/3V	→	K3V
F5V	→	F5.5V	G2/3V	→	G1V	K3V	→	K3V
F5/6V	→	F6V	G3V	→	G1.5V	K3/4V	→	K4V
F6V	→	F6V	G3/5V	→	G4V	K4V	→	K4+V
F6/7V	→	F6.5V	G5V	→	G4.5V	K4/5V	→	K5V
F7V	→	F7.5V	G5/6V	→	G6V	K5V	→	K6-V
F7/8V	→	F8V	G8V	→	G8.5V	K5/M0V	→	K7V
F8V	→	F8.5V				M0V	→	K6.5V
F8/G0V	→	F9V						

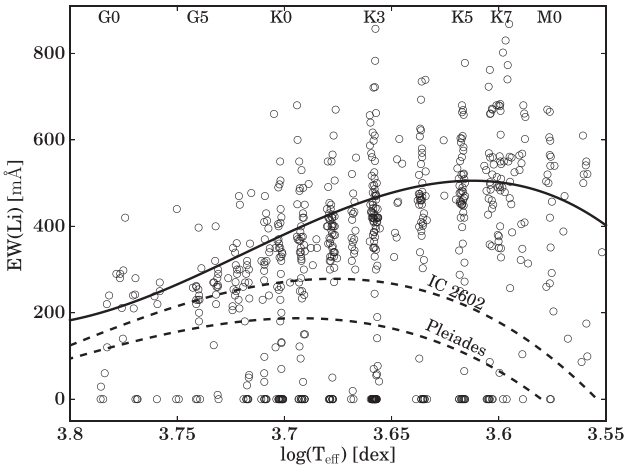

Figure 1. Measured EW(Li) from the 6708 Å line plotted against log ($T_{\rm eff}$) for our X-ray sample. Plotted dashed lines are polynomial fits to data from surveys in IC 2602 (Randich et al. 1997) and the Pleiades (Soderblom et al. 1993; Jones et al. 1996). The location of the EW(Li) for our Sco–Cen candidate members is used to determine the membership indicator in Table 4. Those above the IC 2602 curve are marked 'Y', those above the Pleiades curve are marked 'Y?', while candidates below the Pleiades are marked 'N'. The solid curve is a polynomial fit to the Sco–Cen candidates marked 'Y'; the polynomial coefficients are listed in Table 6.

We compare our EW(Li) measurements at a given $T_{\rm eff}$ to those in nearby open clusters. In Fig. 1 we plot $T_{\rm eff}$ versus EW(Li) for our sample along with data for the young open clusters IC 2602 (Randich et al. 1997) and the Pleiades (Soderblom et al. 1993; Jones, Fischer & Stauffer 1996). Most stars in our sample exhibit much larger EW(Li) at a given $T_{\rm eff}$ than either IC 2602 (∼45 Myr; Dobbie, Lodieu & Sharp 2010) or the Pleiades (∼125 Myr; Stauffer, Schultz & Kirkpatrick 1998). These data suggest that Li is largely undepleted for the ∼10–16 Myr-old stars in Sco–Cen hotter than spectral type ∼K3, but the Li depletion becomes very strong for stars cooler than ∼K3 (∼1.1 $M_{\odot}$). We fit low-order polynomials to the IC 2602 and Pleiades $T_{\rm eff}$ versus EW(Li) data; the polynomial coefficents are listed in Table 6. For our Li-based membership criterion, if the EW(Li) was above the polynomial fit to IC 2602 we marked that star as 'Y' in Table 4; if EW(Li) was below the IC 2602 polynomial fit but above the Pleiades polynomial fit, we marked it as 'Y?', and if the EW(Li) is below the Pleiades polynomial fit we marked it as 'N'. Stars studied in Preibisch & Zinnecker (1999), Köhler et al. (2000) and Krautter et al. (1997) were confirmed as Li-rich but the measurements were not reported. We marked these candidates as 'Y' in Table 4. In total, we marked 482 candidates as 'Y', 153 as 'N', and 38 as 'Y?'.

Table 6. Polynomial fits to Li versus $T_{\rm eff}$ data.

Polynomial coefficient	IC 2602	Pleiades	Sco–Cen
a_0	-1.869522×10^6	-1.639425×10^6	-3.576491×10^6
a_1	1.472855×10^6	1.290057×10^6	2.890342×10^6
a_2	-3.862308×10^5	-3.379855×10^5	-7.778982×10^5
a_3	3.371432×10^4	2.948343×10^4	6.972998×10^4

Note: $EW(Li)[m\,\text{Å}] = a_0 + a_1(\log(T_{\rm eff})) + a_2(\log(T_{\rm eff}))^2 + a_3(\log(T_{\rm eff}))^3$
Polynomial fit is valid from $\log(T_{\rm eff}) = 3.800$ dex to 3.580 dex.

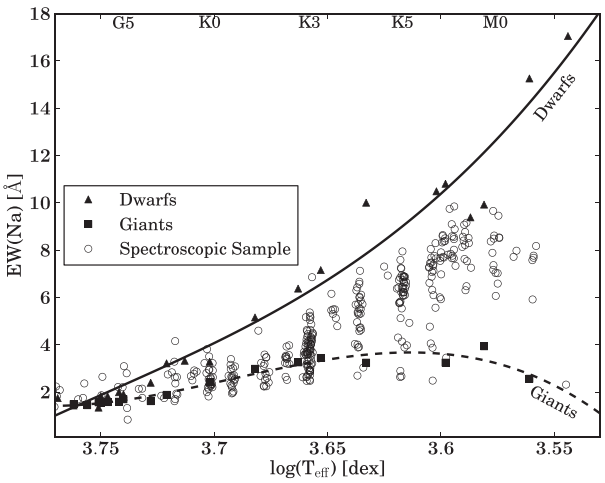

Figure 2. Measured EW(Na) from the Na I doublet at 5889 Å/5896 Å line plotted against $\log(T_{\rm eff})$ for our spectroscopic sample. Plotted are polynomial fits to dwarf and giant spectral standard stars used for classification.

4.3.2 *Surface gravity*

Based on previous nuclear and pre-MS age determinations of the subgroups of Sco–Cen (Mamajek et al. 2002; Pecaut et al. 2012), the low-mass stars in Sco–Cen are expected to be pre-main sequence with surface gravities intermediate between dwarfs and giants. For candidates in our spectroscopic sample we can examine spectral features sensitive to surface gravity, primarily the Na I doublet at 5889 Å/5896 Å. Details on using Na I as a surface gravity indicator for identifying young stars is discussed in detail in Schlieder et al. (2012). The Na I doublet decreases in strength at a given $T_{\rm eff}$ as surface gravity decreases. However, the observed strength of the Na I doublet in subgiants among G-type stars is difficult to distinguish from dwarfs. The differences in the Na I doublet strength between dwarfs and subgiants becomes more useful in mid-K-type spectra, as shown in Fig. 2. For this reason we are fairly conservative in our surface gravity membership criterion, marking G-type stars with luminosity classes of 'IV' with 'Y', 'V' with 'Y?' and 'III' with 'N'. Note that we only use this criterion for stars which we have observed spectroscopically; luminosity classifications from other authors for stars in our parent sample are not used for this criterion. We assigned 345 stars into these two categories, with 300 marked as 'Y?' and 45 marked as 'N'.

4.3.3 *Distances*

As mentioned previously, the majority of our sample lack trigonometric distance estimates. However, if we calculate a kinematic parallax estimate using the best available proper motion, we can then estimate distances for each star in our sample and verify that this lies within the range of expected distances for the association. Stars with discrepant kinematic distances are identified as non-members. We use the results of the membership study of Rizzuto et al. (2011), which makes use of the revised *Hipparcos* trignometric parallaxes (van Leeuwen 2007), to establish our distance criteria. Based on the spatial distribution of their candidate members, Rizzuto et al. (2011) concluded that strict boundaries between the subgroups are somewhat arbitrary, so we do not use distinct kinematic distance criteria for each subgroup. To establish parallax (ϖ) limits based on galactic longitude and latitude (l, b), we fit a plane to the B-type members with membership probabilities >50 per cent from the Rizzuto et al. (2011) study, obtaining:

$$\begin{aligned}\varpi &= (-0.0208 \pm 0.0061) \times (l - \langle l \rangle) \\ &+ (-0.0299 \pm 0.0158) \times (b - \langle b \rangle) \\ &+ (7.7761 \pm 0.0969)\end{aligned}$$

with mean galactic coordinates $\langle l \rangle = 328.^\circ579$, $\langle b \rangle = 13.^\circ261$. The 1σ dispersion in the fit is $\sigma_\varpi \simeq 1.25$ mas. Therefore we model the shape of Sco–Cen with a continuous plane and depth characterized by 1σ dispersion of $\sim$1.25 mas. For our kinematic distance criteria, we mark stars with 'Y' in Table 4 if their kinematic parallaxes are within the 2σ (95 per cent C.L.) dispersion from the plane described above, and 'Y?' if they are between 2σ and 3σ. We mark stars with 'N' if they are beyond 3σ of the dispersion from the plane. This criteria effectively provides different distance limits as a function of galactic longitude and latitude, giving typical 2σ distance limits of 141^{+77}_{-37} pc, 130^{+62}_{-32} pc, and 117^{+49}_{-27} pc for US, UCL and LCC, respectively. 677 stars in our sample have been placed in these categories, with 495 marked as 'Y', 80 as 'Y?', and 102 as 'N'.

4.3.4 *HRD position*

As a final membership check, we place these stars on the H–R diagram using their kinematic distances, which, for this purpose, *assumes* they are comoving with other members in the association. Objects that have H–R diagram positions inconsistent with membership, e.g. below the main sequence, are rejected. Below we discuss the few stars which were Li-rich and fell inside our kinematic distance criteria but were rejected because they had discrepant H–R diagram positions. Two stars were rejected since they fell below the main sequence and two stars were rejected since they were well above the 1 Myr isochrone. Unresolved binarity is insufficient to account for these discrepant positions. Further analysis can be found in Section 4.5.

4.3.5 *Interlopers*

US: HD 144610 is a Li-rich K1IV-III which has a kinematic parallax of $\pi_{\rm kin} = 3.41 \pm 0.69$ mas which is consistent with an H–R diagram position of $\log(T_{\rm eff}) = 3.70 \pm 0.01$, $\log(L/L_\odot) = 1.42 \pm 0.18$, well above the 1 Myr isochrone, so we reject it.

UCL: 2MASS J14301461-4520277 is a Li-rich K3IV(e) which, using the kinematic parallax of $\pi_{\rm kin} = 10.92 \pm 0.92$ mas, has an H–R diagram position well below the main sequence ($\log(T_{\rm eff}) = 3.66 \pm 0.02$, $\log(L/L_\odot) = -0.91 \pm 0.08$), so we reject its membership to UCL. 2MASS J16100321-5026121 is a Li-rich K0III (Torres et al. 2006) which lies well above the 1 Myr isochrone ($\log(T_{\rm eff}) = 3.70 \pm 0.01$, $\log(L/L_\odot) = 1.16 \pm 0.08$), calculated using the kinematic parallax of $\pi_{\rm kin} = 4.19 \pm 0.38$ mas, so we consider a UCL interloper.

LCC: 2MASS J10111521-6620282, lies well below the main sequence, with $\log(T_{\rm eff}) = 3.70 \pm 0.01$, $\log(L/L_\odot) = -0.86 \pm 0.09$, calculated using the predicted kinematic parallax of $\pi_{\rm kin} = 9.63 \pm 0.94$ mas. This is puzzling because it is a Li-rich K0IV, with a proper motion in excellent agreement with membership in LCC. It does not exhibit an infrared excess which could be a signature of an edge-on disc, and the $B-V$ and $V-K_S$ colours are consistent with a negligibly reddened young K0. However, it is ∼0.4 dex underluminous for the main sequence, so we consider it a likely LCC interloper.

4.3.6 Final membership assessment

Though we require the Li, surface gravity indicators, kinematic distance criterion, and H–R diagram criterion to indicate membership, the Li and kinematic distance criteria are the most restrictive and are responsible for identifying most non-members. Stars with 'Y' or 'Y?' in each of the four membership categories have been identified members of Sco–Cen. Though we have made every effort to remove interlopers, our list of candidate members may still contain a few non-members, though it will be dominated by true members. From our current sample, we identify 493 stars as likely members, listed in Table 7. The 180 stars rejected as Sco–Cen members are listed in Table 8. 156 are newly identified young stars.

4.4 Extinction

We estimate the reddening and extinction for Sco–Cen members using the spectral type-intrinsic colour sequence for pre-MS stars described in Pecaut & Mamajek (2013). These intrinsic colours are calibrated using low-mass members of nearby moving groups which have negligible extinction, and bracket the age range of the Sco–Cen subgroups (5–30 Myr). Many of the stars in our sample have very low reddening, and where we obtained a non-physical negative extinction we set the extinction to zero. We used a total-to-selective extinction of $R_V = 3.1$ and calculated $E(B-V)$, $E(V-J)$, $E(V-H)$, and $E(V-K_S)$ with $A_J/A_V = 0.27$, $A_H/A_V = 0.17$, $A_{K_S}/A_V = 0.11$ (Fiorucci & Munari 2003) which allowed us to estimate extinctions to each star individually using as many as four different colours. We adopted the median A_V, and adopted the standard deviation of the A_V values as a conservative estimate of their uncertainty. For the stars which lack reliable V band photometry, we estimate their extinctions using $E(J-K_S)$. Our extinction estimates are listed in Table 7.

4.5 H–R diagram for Sco–Cen members

We place our Sco–Cen members on a theoretical H–R diagram in order to compare with theoretical models and obtain individual isochronal age estimates. We adopt the effective temperature scale ($T_{\rm eff}$) and bolometric correction (BC_V) scale from the Pecaut & Mamajek (2013) study,[5] which was constructed specifically for 5–30 Myr old pre-MS stars. This $T_{\rm eff}$ and BC_V scale was derived by fitting the spectral energy distributions of members of young, nearby

[5] Pecaut & Mamajek (2013) adopted an absolute bolmetric magnitude for the Sun of $M_\odot = 4.755$ mag, ∼0.015 mag higher than the recently drafted IAU bolometric magnitude scale (2015 IAU resolution B2). Thus the BC scale in Pecaut & Mamajek (2013) should be shifted down by ∼0.02 mag to conform to the IAU scale. The luminosity estimates in this present work are on the 2015 IAU scale.

Table 7. Stellar properties for Sco–Cen members.

ID	2MASS	Grp.	SpT	Ref.	EW(Hα) (Å)	Ref.	A_V (mag)	$\pi_{\rm kin}$ (mas)	$\log(T_{\rm eff})$ (dex)	$\log(L/L_\odot)$ (dex)	Age (Myr)	Mass ($M_\odot$)	Disc type	Other name
1	10065573-6352086	LCC	K0Ve	T06	0.0	T06	0.16 ± 0.04	7.54 ± 0.83	3.702 ± 0.009	-0.059 ± 0.097	14	1.1		TYC 8951-289-1
2	10092184-6736381	LCC	K1IV(e)	PM	−0.2	PM	0.00 ± 0.10	7.03 ± 0.76	3.692 ± 0.012	-0.334 ± 0.096	29	0.9		TYC 9210-1484-1
3	10313710-6901587	LCC	K2.5IV(e)	PM	−0.1	PM	0.00 ± 0.13	6.91 ± 0.72	3.668 ± 0.019	-0.380 ± 0.095	21	0.9		
4	10334180-6413457	LCC	K2.5IV(e)	PM	0.0	PM	0.00 ± 0.15	5.29 ± 0.85	3.668 ± 0.019	-0.077 ± 0.143	7	1.2		V542 Car
5	10412300-6940431	LCC	G8Ve	T06	0.0	T06	0.00 ± 0.02	11.05 ± 0.97	3.717 ± 0.007	-0.250 ± 0.078	33	0.9		TYC 9215-1181-1

EW(Hα)< 0 denotes emission, EW(Hα)> 0 denotes absorption. We report the Houk type for the star 16102888-2213477 = HD 145208 (G5V), but internally use the $T_{\rm eff}$ and BC for the equivalent Gray type (G4.5V) in our calculations. See Table 5 for more information.
References – (PM) – This work; (G67) – Garrison (1967); (F87) – Finkenzeller & Basri (1987); (Ho88) – Houk & Smith-Moore (1988); (W94) – Walter et al. (1994); (H94) – Hughes et al. (1994); (W97) – Wichmann et al. (1997); (K97) – Krautter et al. (1997); (P98) – Preibisch et al. (1998); (P99) – Preibisch & Zinnecker (1999); (W99) – Wichmann et al. (1999); (K00) – Köhler et al. (2000); (P01) – Preibisch et al. (2001); (M02) – Mamajek et al. (2002); (P02) – Preibisch et al. (2002); (Z01) – Zuckerman et al. (2001); (T06) – Torres et al. (2006); (R06) – Riaz et al. (2006); (C06) – Carpenter et al. (2006); (W07) – White et al. (2007); (M11) – Müller et al. (2011); (D12) – Dahm, Slesnick & White (2012); (A) – measured from spectrum downloaded from the ESO archive, programme 083.A-9003(A); (B) – measured from spectrum downloaded from the ESO archive, programme 081.C-0779(A).
Only the first five rows are shown; this table is available in its entirety in the electronic version of the journal.

Table 8. Objects rejected as Sco–Cen members.

2MASS	SpT	Ref.	Rejection reason	Other names
10004365-6522155	G3V	PM	μ	
10111521-6620282	K0IV	PM	HRD position	
10293275-6349156	K1IV	PM	μ	TYC 8964-165-1
10342989-6235572	G7Ve	PM	μ	HD 307772
10441393-6446273	K1V(e)	PM	μ	HD 307960

References– (PM) – This work; (K97) – Krautter et al. (1997); (P98) – Preibisch et al. (1998); (K00) – Köhler et al. (2000); (M02) – Mamajek et al. (2002); (T06) – Torres et al. (2006).
Only the first five rows are shown; this table is available in its entirety in the electronic version of the journal.

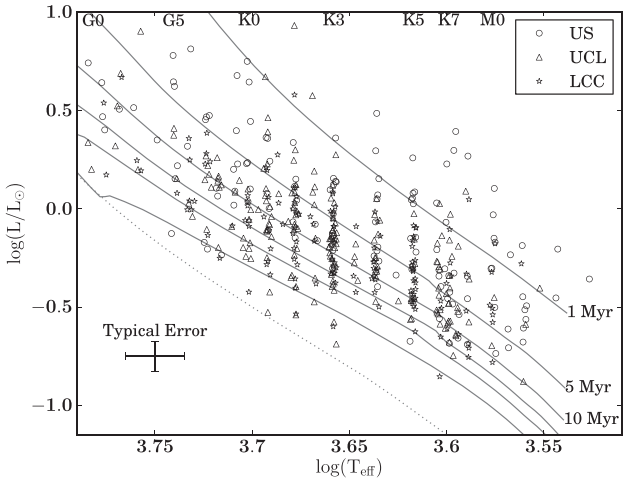

Figure 3. H–R diagram for X-ray selected Sco–Cen members with J–$K_S > 0.50$ as described in the text. Circles, triangles and star symbols are US, UCL and LCC candidate members, respectively. Plotted for comparison are 5, 10, 15, 20 and 30 Myr isochrones from Dotter et al. (2008). Artificial scatter of $\delta T_{\rm eff} = \pm 0.001$ dex has been introduced for plotting purposes.

moving groups to the BT-Settl theoretical atmospheric models (Allard, Homeier & Freytag 2012). Though this $T_{\rm eff}$ and BC scale is dependent on model atmospheres, the method used to develop the resultant $T_{\rm eff}$ scale is in good agreement with $T_{\rm eff}$ values derived from angular diameter measurements (e.g. Boyajian et al. 2012). We combine our individual extinction estimates together with our kinematic parallaxes and 2MASS J-band magnitudes to estimate the bolometric luminosities of our stars and place them on a theoretical H–R diagram. We compare our data to the pre-MS models of Dotter et al. (2008) in Fig. 3.

There is considerable scatter in the H–R diagram so we construct empirical isochrones by plotting the median luminosity along the H–R diagram. Though there is some scatter, the relative age rank of the three groups is consistent with that found in Mamajek et al. (2002), Preibisch & Mamajek (2008), Pecaut et al. (2012); from oldest to youngest: LCC, UCL and US, with UCL and LCC approximately coeval. The other striking feature of the empirical isochrones is the mass-dependent age trend. The lower mass stars appear younger against the theoretical isochrones than the higher mass stars. This is the same mass-dependent age trend seen in other studies (e.g. Hillenbrand 1997; Hillenbrand, Bauermeister & White 2008; Bell et al. 2012, 2013, 2014). The likely origin of the mass-dependent age trend is difficulties in handling convection with magnetic fields

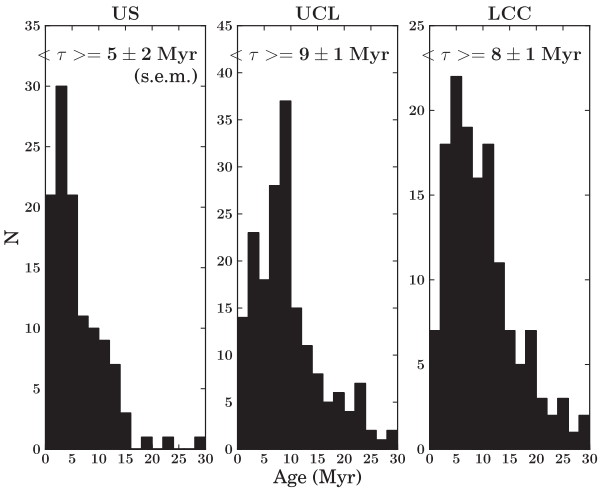

Figure 4. Distribution of raw isochronal ages obtained for the Sco–Cen members of our sample using the Dotter et al. (2008) evolutionary models.

in young, low-mass stars in the evolutionary models, perhaps due to missing physics (see e.g. Feiden 2016). At an age of 10 Myr and 15 Myr, our observational uncertainties yield individual age uncertainties of ±3 Myr and ±4 Myr, respectively.

4.6 Ages

The presence of massive stars in OB associations also allows for the opportunity for a comparison of ages obtained through different parts of the H–R diagram. As massive stars burn through their nuclear fuel, they will expand and leave the main sequence. At the same time, the pre-main-sequence members of the OB association will be contracting towards the main sequence. The evolutionary models will predict ages for each of these segments of the H–R diagram, but different aspects of stellar physics are important in each of these segments. In this section, we examine the ages for both the low-mass pre-MS stars as well as the massive main sequence turn-off stars.

4.6.1 Pre-MS ages

We estimate individual ages for our pre-MS Sco–Cen members by linearly interpolating between theoretical model isochrones. We use the Dartmouth models (Dotter et al. 2008), the Pisa models (Tognelli, Prada Moroni & Degl'Innocenti 2011), the PARSEC models (Chen et al. 2014), and the Exeter/Lyon models (Baraffe et al. 2015). These models each assume slightly different stellar compositions, but are each calibrated to reproduce the H–R diagram position of the Sun at its current age. The Dartmouth evolutionary models adopt the Grevesse & Sauval (1998) solar composition with a protosolar He fraction of Y=0.2740, while the Pisa evolutionary models adopt the Asplund, Grevesse & Sauval (2005) solar composition with a protosolar He fraction of Y = 0.2533. The PARSEC models adopt the Caffau et al. (2008, 2009) solar abundances with a initial He fraction of Y = 0.284, whereas the Exeter/Lyon models use the Caffau et al. (2011) solar abundances, Y = 0.271. The distributions of ages we obtain with the Dartmouth evolutionary models is shown in Fig. 4. We obtain median ages of 5 ± 2 Myr, 9 ± 1 Myr and 8 ± 1 Myr (standard error of the median) for US, UCL and LCC, respectively. Surprisingly, these ages are half the mean ages obtained from the F-type members of Sco–Cen (Pecaut et al. 2012).

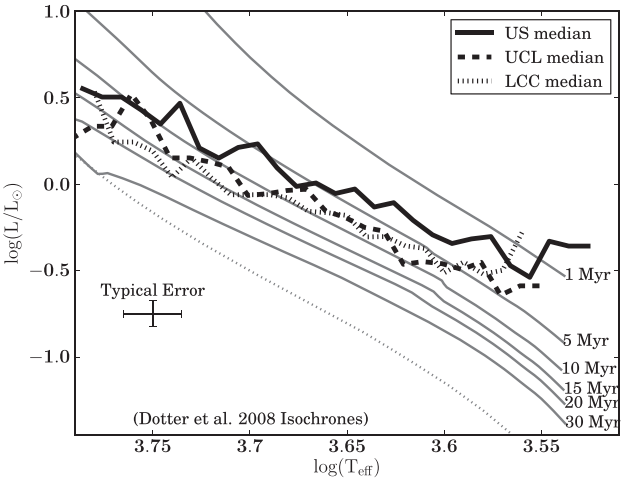

Figure 5. H–R diagram with empirical isochrones for US (solid), UCL (dashed) and LCC (dotted). All three subgroups exhibit a mass-dependent age trend.

Given the large $T_{\rm eff}$-dependent trend with age (Fig. 5), we decide against adopting mean subgroup ages based on the K- and M-type members of Sco–Cen. A detailed discussion of our reasoning is available in Section 5.1.

In order to extract useful age estimates for the subgroups, we re-examine the G-type pre-MS ages as well as the main-sequence turn-off ages. We do this for two reasons, other than the obvious desire to quote reliable mean ages. The first reason is that estimating realistic intrinsic age spreads requires a reliable age as free of systematic uncertainties as possible. We use Monte Carlo simulations to constrain our intrinsic age spreads, taking into account realistic binarity statistics and observational uncertainties, the details of which are described in Section 4.7. Because isochrones evenly spaced in age will not generally be evenly spaced in luminosity, a large intrinsic spread in luminosity at a young age could still be consistent with a small age spread, whereas the same intrinsic spread in luminosity at an older age would imply a larger intrinsic age spread. The second reason we reevaluate the G-type ages and nuclear ages is that updated $T_{\rm eff}$ and bolometric corrections (BCs) have been made available since the ages were last estimated in Mamajek et al. (2002). For the hot stars, Nieva (2013) used modern non-local thermodynamic equilibrium (NLTE) spectral synthesis models to re-evaluate the $T_{\rm eff}$ and BC scale for the massive OB stars (34 000 K > $T_{\rm eff}$ > 15 800 K). Their results for dwarfs and subgiants are 1500–6000 K hotter than the scale of Napiwotzki, Schoenberner & Wenske (1993) that was adopted in the study of Mamajek et al. (2002). As previously mentioned, Pecaut & Mamajek (2013) have constructed an updated $T_{\rm eff}$ and BC scale applicable to the Sco–Cen G-type stars. Both of these studies should allow us to place Sco–Cen members on the H–R diagram with reduced systematic uncertainties.

4.6.2 Isochronal ages for G-type pre-MS stars

To estimate the ages of the G-type pre-MS stars, we collect the G-type members from this study together with those in Walter et al. (1994), Preibisch & Zinnecker (1999), Mamajek et al. (2002), and Preibisch & Mamajek (2008). We supplement this with G-type stars studied in Torres et al. (2006) in the Sco–Cen field which are Li-rich and have proper motions consistent with membership; G-type stars identified as members here conform to the membership criteria discussed in Section 4.3. The stellar properties for these stars are listed in Table 7 and Table 9, together with the median mass and age obtained through a comparison of their H–R diagram positions with the evolutionary models of Dotter et al. (2008), Tognelli et al. (2011), Chen et al. (2014), and Baraffe et al. (2015).

4.6.3 Isochronal turn-off ages for massive stars

To estimate nuclear ages, we collect membership lists for the most massive stars from de Zeeuw et al. (1999), Mamajek et al. (2002), Rizzuto et al. (2011) and Pecaut et al. (2012). We collect Stromgren *ubvyβ* and Johnson *UBV* photometry from Hauck & Mermilliod (1998) and Mermilliod & Mermilliod (1994). We estimate the extinction towards each early B-type member with both the Q-method (Johnson & Morgan 1953; updated in Pecaut & Mamajek 2013) using Johnson *UBV* photometry, and the prescription of Shobbrook (1983), using Stromgren *ubvyβ* photometry. For all the massive stars these two methods give similar A_V within the uncertainties, so we adopt the mean value. We calculate the $T_{\rm eff}$ and BC$_V$ for each star using the calibrations with Q, $[u-b]$, $[c1]$ and β in Nieva (2013); we adopt the median $T_{\rm eff}$ when available. We note that the calibrations derived by Nieva (2013) give systematically hotter $T_{\rm eff}$ than the calibrations of Napiwotzki et al. (1993) and Balona (1994), which were used in Mamajek et al. (2002) and Pecaut et al. (2012), respectively, in the most recent estimation of Sco–Cen nuclear ages. Because of this we expect to obtain younger turn-off ages than previously estimated.

Our stellar parameters for the main-sequence turn-off in Sco–Cen are listed in Table 10, along with an individual age estimate of each object from a comparison the rotating tracks of Ekström et al. (2012), rotating at $v_{\rm eq} = 0.4 v_{\rm crit}$, with the H–R diagram position of the stars. A plot of the main-sequence turn-off for all three subgroups is shown in Fig. 6. To estimate the turn-off age of Upper Sco we use τ Sco, ω Sco, σ Sco, β^1 Sco, π Sco, and δ Sco. We obtain a median turn-off age for US of ∼7 Myr. We concur with de Zeeuw et al. (1999) that o Sco is unlikely to be a US member.[6] For Upper Centaurus-Lupus, we use μ Cen, δ Lup, α Lup, μ^1 Sco, μ^2 Sco, β Lup, γ Lup, ν Cen, η Cen, η Lup, ϕ Cen, ε Lup, κ Cen, and HR 6143. We obtain a median age for UCL of ∼19 Myr. For Lower Centaurus-Crux, we use α^1 Cru, β Cru, β Cen, δ Cru and α Mus. We obtain a median age of ∼11 Myr. Note that these are all in the southern part of LCC, for which Preibisch & Mamajek (2008) estimated ∼12 Myr. There are no turn-off stars in the northern part of LCC, the hottest of which appear to be older (∼20 Myr). Our nuclear median subgroup ages are summarized in Table 11.

We summarize our derived nuclear, F-type pre-MS and G-type pre-MS ages in Table 11 with our adopted values for each subregion.

4.7 Intrinsic age spreads

The H–R diagram positions of Sco–Cen members have a large degree of scatter, and hence a large apparent scatter in inferred ages. Some of this scatter is due to observational uncertainties and unresolved multiplicity, but some scatter may be due to true age spreads within the subgroups. Previous studies have found very small intrinsic age spreads in US, but larger age spreads in UCL and LCC

[6] o Sco is an A5II (Gray & Garrison 1989) with a parallax of 3.71 ± 0.54 mas (van Leeuwen 2007). Its evolutionary status, proper motion, and distance (∼270 pc) are inconsistent with membership in Upper Sco.

Table 9. Stellar parameters for Sco–Cen G-type stars.

Object Name	2MASS	Spectral type	Ref.	Region	A_V (mag)	$\log(T_{\rm eff})$ (dex)	$\log(L/L_\odot)$ (dex)	Age (Myr)	Mass ($M_\odot$)
TYC 9216-0524-1	10495605-6951216	G8V	T06	LCC	0.00 ± 0.05	3.717 ± 0.007	-0.382 ± 0.069	48	0.9
TYC 9212-1782-1	10594094-6917037	G6V	T06	LCC	0.00 ± 0.02	3.732 ± 0.008	0.428 ± 0.085	6	1.6
CD-48 6632	11350376-4850219	G7V	T06	LCC	0.00 ± 0.15	3.709 ± 0.008	0.048 ± 0.075	11	1.2
HIP 57524	11472454-4953029	G0V	PM	LCC	0.18 ± 0.04	3.782 ± 0.004	0.413 ± 0.061	17	1.3
CPD-63 2126	12041439-6418516	G8V	T06	LCC	0.00 ± 0.04	3.717 ± 0.007	0.012 ± 0.071	15	1.2
MML 3	12044888-6409555	G1V	PM	LCC	0.38 ± 0.06	3.776 ± 0.007	0.484 ± 0.084	14	1.3
HIP 58996	12054748-5100121	G1V	PM	LCC	0.15 ± 0.04	3.776 ± 0.007	0.407 ± 0.057	16	1.3
MML 7	12113815-7110360	G5V	PM	LCC	0.23 ± 0.02	3.740 ± 0.009	0.338 ± 0.067	10	1.4
HIP 59854	12162783-5008356	G1V	PM	LCC	0.31 ± 0.05	3.776 ± 0.007	0.531 ± 0.061	13	1.4
MML 14	12211648-5317450	G1V	PM	LCC	0.39 ± 0.05	3.776 ± 0.007	0.433 ± 0.067	15	1.3
MML 17	12223322-5333489	G0V	PM	LCC	0.24 ± 0.03	3.782 ± 0.004	0.448 ± 0.066	16	1.3
CD-54 4763	12242065-5443540	G5V	T06	LCC	1.00 ± 0.39	3.740 ± 0.009	0.598 ± 0.085	5	1.8
HIP 60885	12284005-5527193	G0V	PM	LCC	0.20 ± 0.04	3.782 ± 0.004	0.482 ± 0.057	15	1.3
HIP 60913	12290224-6455006	G2V	PM	LCC	0.44 ± 0.04	3.769 ± 0.009	0.498 ± 0.060	12	1.4
MML 29	13023752-5459370	G0V	PM	LCC	0.44 ± 0.10	3.782 ± 0.004	0.257 ± 0.072	23	1.2
HIP 63847	13050530-6413552	G4V	PM	LCC	0.19 ± 0.03	3.750 ± 0.009	0.320 ± 0.058	12	1.3
CD-59 4629	13132810-6000445	G3V	T06	LCC	0.10 ± 0.04	3.759 ± 0.009	0.289 ± 0.068	16	1.2
MML 32	13175694-5317562	G0V	PM	LCC	0.75 ± 0.14	3.782 ± 0.004	0.616 ± 0.102	12	1.5
MML 33	13220446-4503231	G0V	PM	LCC	0.16 ± 0.05	3.782 ± 0.004	0.220 ± 0.057	25	1.2
HIP 65423	13243512-5557242	G3V	T06	LCC	0.00 ± 0.02	3.759 ± 0.009	0.332 ± 0.057	14	1.3
HIP 65517	13254783-4814577	G1V	PM	LCC	0.23 ± 0.05	3.776 ± 0.007	0.104 ± 0.053	28	1.1
MML 35	13342026-5240360	G0V	PM	LCC	0.38 ± 0.07	3.782 ± 0.004	0.478 ± 0.058	15	1.3
MML 37	13432853-5436434	G0V	PM	LCC	0.33 ± 0.04	3.782 ± 0.004	0.213 ± 0.053	25	1.2
HIP 67522	13500627-4050090	G0V	PM	UCL	0.23 ± 0.04	3.782 ± 0.004	0.233 ± 0.063	24	1.2
MML 42	14160567-6917359	G1V	PM	LCC	0.17 ± 0.02	3.776 ± 0.007	0.262 ± 0.059	22	1.2
HIP 71178	14332578-3432376	G9IV	PM	UCL	0.12 ± 0.02	3.709 ± 0.008	0.031 ± 0.057	12	1.2
MML 49	14473176-4800056	G7IV	PM	UCL	0.00 ± 0.04	3.723 ± 0.007	-0.109 ± 0.067	24	1.0
MML 52	14571962-3612274	G3V	PM	UCL	0.43 ± 0.03	3.759 ± 0.009	0.305 ± 0.062	15	1.3
MML 56	15011155-4120406	G0V	PM	UCL	0.32 ± 0.04	3.782 ± 0.004	0.613 ± 0.068	12	1.5
MML 57	15015882-4755464	G0V	PM	UCL	0.24 ± 0.04	3.782 ± 0.004	0.333 ± 0.071	20	1.2
MML 61	15125018-4508044	G2V	PM	UCL	0.31 ± 0.04	3.769 ± 0.009	0.165 ± 0.082	24	1.1
MML 62	15180174-5317287	G6V	PM	UCL	0.31 ± 0.01	3.732 ± 0.008	0.041 ± 0.063	18	1.1
TYC 8298-1675-1	15193702-4759341	G9IV	T06	UCL	0.00 ± 0.02	3.709 ± 0.008	-0.336 ± 0.069	38	0.9
HIP 75483	15251169-4659132	G9V	T06	UCL	0.00 ± 0.16	3.709 ± 0.008	-0.220 ± 0.067	27	1.0
HIP 75924	15302626-3218122	G3V	PM	UCL	0.33 ± 0.11	3.759 ± 0.009	0.572 ± 0.063	8	1.6
HIP 76472	15370466-4009221	G0V	PM	UCL	0.52 ± 0.03	3.782 ± 0.004	0.560 ± 0.060	13	1.4
MML 69	15392440-2710218	G5V	PM	UCL	0.34 ± 0.11	3.740 ± 0.009	0.451 ± 0.070	7	1.6
HIP 77135	15445769-3411535	G3V	PM	UCL	0.43 ± 0.04	3.759 ± 0.009	0.066 ± 0.064	27	1.1
HIP 77144	15450184-4050310	G0V	PM	UCL	0.19 ± 0.10	3.782 ± 0.004	0.407 ± 0.060	18	1.3
HIP 77190	15454266-4632334	G5IV	T06	UCL	0.00 ± 0.03	3.740 ± 0.009	-0.200 ± 0.059	39	0.9
MML 72	15465179-4919048	G7V	PM	UCL	0.13 ± 0.04	3.723 ± 0.007	0.136 ± 0.064	12	1.3
HIP 77656	15511373-4218513	G7V	PM	UCL	0.00 ± 0.01	3.723 ± 0.007	0.339 ± 0.062	7	1.6
TYC 7846-1538-1	15532729-4216007	G2	T06	UCL	0.88 ± 0.35	3.769 ± 0.009	0.382 ± 0.067	15	1.3
HD 142361	15545986-2347181	G2IV	W94	US	0.46 ± 0.12	3.769 ± 0.009	0.314 ± 0.070	18	1.2
HD 142506	15554883-2512240	G3	P99	US	0.40 ± 0.03	3.759 ± 0.009	0.432 ± 0.076	11	1.4
HIP 78133	15571468-4130205	G3V	T06	UCL	0.00 ± 0.07	3.759 ± 0.009	0.063 ± 0.066	27	1.1
HD 143099	15595826-3824317	G0V	T66	UCL	0.00 ± 0.05	3.782 ± 0.004	0.449 ± 0.066	16	1.3
CD-24 12445	16000078-2509423	G0	P99	US	0.37 ± 0.17	3.782 ± 0.004	0.256 ± 0.074	23	1.2
TYC 7333-1260-1	16010792-3254526	G1V	T06	UCL	0.21 ± 0.06	3.776 ± 0.007	0.371 ± 0.061	17	1.2
MML 75	16010896-3320141	G5IV	PM	UCL	0.81 ± 0.05	3.740 ± 0.009	0.480 ± 0.066	6	1.6
HIP 78483	16011842-2652212	G2IV	T06	US	0.33 ± 0.07	3.769 ± 0.009	0.710 ± 0.077	8	1.7
HIP 78581	16024415-3040013	G1V	H82	US	0.08 ± 0.05	3.776 ± 0.007	0.353 ± 0.069	18	1.2
HIP 79462	16125533-2319456	G2V	H88	US	0.53 ± 0.13	3.769 ± 0.009	0.887 ± 0.077	5	2.0
MML 82	16211219-4030204	G8V	PM	UCL	0.00 ± 0.07	3.717 ± 0.007	0.204 ± 0.063	8	1.4
MML 83	16232955-3958008	G1V	PM	UCL	0.48 ± 0.12	3.776 ± 0.007	0.212 ± 0.084	24	1.1
HIP 80320	16235385-2946401	G3IV	T06	US	0.05 ± 0.02	3.759 ± 0.009	0.459 ± 0.071	11	1.4
HIP 80535	16262991-2741203	G0V	H82	US	0.00 ± 0.03	3.782 ± 0.004	0.727 ± 0.071	9	1.6
HIP 80636	16275233-3547003	G0V	PM	UCL	0.36 ± 0.05	3.782 ± 0.004	0.563 ± 0.060	13	1.4
HIP 81380	16371286-3900381	G2V	PM	UCL	0.34 ± 0.08	3.769 ± 0.009	0.798 ± 0.069	6	1.8
HIP 81447	16380553-3401106	G0V	PM	UCL	0.12 ± 0.16	3.782 ± 0.004	0.814 ± 0.065	8	1.7

G-type stars not included in Table 7. Ages and masses were estimated using the median of Baraffe et al. (2015), Chen et al. (2014), Tognelli et al. (2011) and Dotter et al. (2008) evolutionary models. We report the Houk types for the stars HIP 78581 (G1V), HIP 79462 (G2V) and HIP 80535 (G0V), but adopt the $T_{\rm eff}$ and BC for the equivalent Gray types in our calculations. See Table 5 for the conversions and Section 4.1 for discussion.
Spectral type references: (PM) This work; (T06) Torres et al. (2006); (W94) Walter et al. (1994); (P99) Preibisch & Zinnecker (1999); (T66) Thackeray (1966); (H82) Houk (1982); (Ho88) Houk & Smith-Moore (1988).
Adopted median subgroup ages (Table 11) are preferable to uncertain individual ages listed above.

Table 10. Stellar parameters for Sco–Cen main-sequence turn-off stars.

Object name	Spectral type	Ref.	Region	A_V (mag)	$\log(T_{\rm eff})$ (dex)	$\log(L/L_\odot)$ (dex)	Age Myr
τ Sco	B0V	1	US	0.109 ± 0.029	4.505 ± 0.004	4.351 ± 0.125	1
δ Sco	B0.5IV	1	US	0.432 ± 0.025	4.479 ± 0.030	4.664 ± 0.133	7
β^1 Sco	B0.5V	1	US	0.547 ± 0.031	4.464 ± 0.021	4.394 ± 0.096	7
σ Sco	B1III	1	US	1.203 ± 0.009	4.466 ± 0.028	5.019 ± 0.126	8
ω Sco	B1V	1	US	0.647 ± 0.013	4.454 ± 0.016	4.013 ± 0.048	1
π Sco	B1V+B2:V:	1	US	0.204 ± 0.005	4.437 ± 0.030	4.411 ± 0.119	10
1 Sco	B1.5Vn	1	US	0.462 ± 0.008	4.355 ± 0.016	3.490 ± 0.049	5
ν Sco	B2IV	1	US	0.756 ± 0.021	4.341 ± 0.012	3.800 ± 0.100	23
β^2 Sco	B2IV-V	1	US	0.538 ± 0.025	4.340 ± 0.018	3.190 ± 0.130	<1
ρ Sco	B2IV-V	1	US	0.081 ± 0.033	4.335 ± 0.032	3.561 ± 0.074	18
13 Sco	B2V	1	US	0.112 ± 0.005	4.300 ± 0.022	3.234 ± 0.052	15
α Lup	B1.5III	2	UCL	0.094 ± 0.009	4.360 ± 0.014	4.237 ± 0.037	19
δ Lup	B1.5IV	2	UCL	0.030 ± 0.017	4.384 ± 0.033	4.455 ± 0.145	15
μ^1 Sco	B1.5IV	2	UCL	0.060 ± 0.010	4.363 ± 0.030	4.011 ± 0.142	19
η Cen	B1.5Vn	2	UCL	0.021 ± 0.021	4.349 ± 0.021	3.796 ± 0.024	21
β Lup	B2III	2	UCL	0.045 ± 0.008	4.354 ± 0.018	3.891 ± 0.043	20
HR 6143	B2III	2	UCL	0.161 ± 0.016	4.326 ± 0.019	3.580 ± 0.050	23
ν Cen	B2IV	2	UCL	0.025 ± 0.003	4.386 ± 0.031	3.772 ± 0.070	8
μ^2 Sco	B2IV	2	UCL	0.051 ± 0.014	4.356 ± 0.033	3.724 ± 0.072	17
ϕ Cen	B2IV	2	UCL	0.000 ± 0.019	4.345 ± 0.030	3.666 ± 0.069	19
γ Lup	B2IV	2	UCL	0.018 ± 0.003	4.337 ± 0.030	3.880 ± 0.085	24
κ Cen	B2IV	2	UCL	0.015 ± 0.008	4.306 ± 0.029	3.591 ± 0.082	30
υ^1 Cen	B2IV-V	2	UCL	0.009 ± 0.020	4.318 ± 0.027	3.410 ± 0.062	18
ϵ Lup	B2IV-V	2	UCL	0.035 ± 0.022	4.277 ± 0.029	3.692 ± 0.114	>30
μ Cen	B2IV-Ve	2	UCL	0.257 ± 0.030	4.456 ± 0.040	4.163 ± 0.092	4
χ Cen	B2V	2	UCL	0.018 ± 0.012	4.302 ± 0.025	3.342 ± 0.061	23
η Lup	B2.5IV	2	UCL	0.003 ± 0.003	4.352 ± 0.031	3.685 ± 0.070	17
τ Lib	B2.5V	2	UCL	0.028 ± 0.006	4.242 ± 0.031	3.218 ± 0.071	>30
θ Lup	B2.5Vn	2	UCL	0.031 ± 0.020	4.248 ± 0.035	3.106 ± 0.092	>30
HR 5471	B3V	2	UCL	0.045 ± 0.002	4.251 ± 0.029	3.034 ± 0.064	>30
HR 5378	B7IIIp	2	UCL	0.038 ± 0.012	4.273 ± 0.019	3.152 ± 0.049	28
β Cru	B0.5III	2	LCC	0.077 ± 0.006	4.458 ± 0.014	4.414 ± 0.079	8
α^1 Cru	B0.5IV	2	LCC	0.018 ± 0.041	4.436 ± 0.038	4.664 ± 0.094	11
β Cen	B1III	2	LCC	0.075 ± 0.031	4.428 ± 0.022	4.905 ± 0.072	11
ξ^2 Cen	B1.5V	2	LCC	0.061 ± 0.005	4.308 ± 0.029	3.329 ± 0.069	18
HR 4618	B2IIIne	2	LCC	0.043 ± 0.009	4.247 ± 0.010	3.058 ± 0.075	>30
δ Cru	B2IV	2	LCC	0.000 ± 0.007	4.403 ± 0.025	3.838 ± 0.056	6
α Mus	B2IV-V	2	LCC	0.015 ± 0.015	4.351 ± 0.024	3.696 ± 0.054	18
μ^1 Cru	B2IV-V	2	LCC	0.067 ± 0.009	4.297 ± 0.025	3.309 ± 0.057	24
σ Cen	B2V	2	LCC	0.060 ± 0.022	4.303 ± 0.032	3.358 ± 0.073	23
ζ Cru	B2.5V	2	LCC	0.021 ± 0.021	4.246 ± 0.025	3.048 ± 0.070	>30

Ages were estimated using the Ekström et al. (2012) rotating evolutionary models with solar abundances. Spectral type references: (1) Hiltner, Garrison & Schild (1969); (2) Garrison (1967).

(Mamajek et al. 2002; Preibisch et al. 2002; Slesnick et al. 2006; Preibisch & Mamajek 2008; Pecaut, Mamajek & Bubar 2012). We perform Monte Carlo simulations in order to model the scatter caused by the observational uncertainties, the effects of unresolved binarity, and an intrinsic age spread. We create many populations of 10^4 simulated members with a Gaussian distribution of ages, assuming a Kroupa (2001) initial mass function (IMF), a spot filling factor from 0 per cent to 50 per cent, a multiplicity fraction of 0.44 and companion mass ratio distribution given by a flat power-law distribution with $\gamma = 0.3$ (using multiplicity properties for $0.7\ M_\odot \lesssim M_* \lesssim 1.3\ M_\odot$ Population I main-sequence stars as summarized in Duchêne & Kraus 2013 and Raghavan et al. 2010). To create the simulated population, each star is assigned a mass and an age, determined to be either binary or single, assigned a companion mass if binary, and assigned a spot coverage ratio from a random uniform distribution ranging from 0 per cent to 50 per cent, which alters its H–R diagram position according to the Somers & Pinsonneault (2015) correction factors. We then introduce dispersion in their H–R diagram positions with the median observational uncertainties from our sample. This is designed to simulate a population with a given mean age, an intrinsic age spread, the effects of unresolved binarity, cool spots, and observational uncertainties. Following Hillenbrand et al. (2008), we compare the observed luminosity spreads around the empirical isochrones in Sco–Cen members to the simulated luminosity spreads. We emphasize that in this comparison, we only compare the distributions of luminosities around the median. We do not compare the median ages obtained since we observe a mass-dependent age trend. However, unlike Hillenbrand et al. (2008), we only model star formation with a given mean age and intrinsic (Gaussian) spread, rather than consider accelerating star formation or other distributions of ages.

We compare our observed luminosity spread with the luminosity spread from the simulations using a Anderson–Darling goodness-of-fit test (e.g. Hou et al. 2009), and adopt the age spread which best

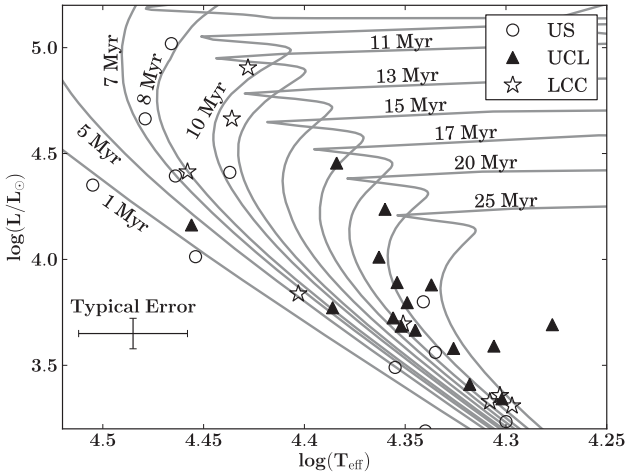

Figure 6. Theoretical H–R diagram for the upper main-sequence members of Sco–Cen with isochrones from the rotating evolutionary models of Ekström et al. (2012) with solar metallicity ($Z = 0.014$).

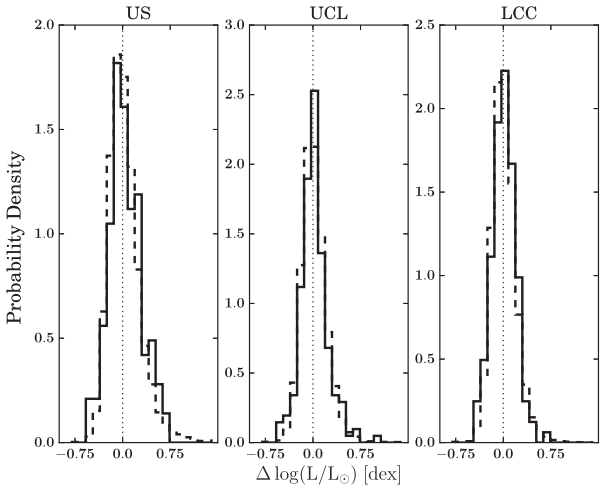

Figure 7. Observed luminosity spreads around the empirical isochrone (solid line) compared with the same for a simulated population (dashed line). The simulations used mean ages of 10 Myr, 16 Myr and 15 Myr for US, UCL, and LCC, respectively. We obtained best-fitting intrinsic age spreads of ±7 Myr, ±7 Myr, ±6 Myr for US, UCL and LCC, shown above with simulations made with the Baraffe et al. (2015) evolutionary models.

Table 11. Adopted subgroup ages.

Method	US (Myr)	UCL (Myr)	LCC (Myr)
MS turn-off	7 ± 2	19 ± 2	11 ± 2
G-type pre-MS	10 ± 1	15 ± 1	15 ± 1
F-type pre-MS[a]	13 ± 1	16 ± 1	17 ± 1
Adopted	10 ± 3	16 ± 2	15 ± 3

Uncertainties reported above are the standard error of the mean which represents the uncertainty in how well the mean value is characterized; these numbers do not represent the spread in ages. Median ages are derived considering the B-type main-sequence turn-off, the F-type pre-MS turn-on and the pre-MS G-type stars in each subgroup.
[a] Adopted F-type Pre-MS ages from Pecaut et al. (2012).

Table 12. Subregion intrinsic age spreads.

Evolutionary models	US at 10 Myr (Myr)	UCL at 16 Myr (Myr)	LCC at 15 Myr (Myr)
Exeter/Lyon	±8	±8	±6
Parsec	±6	±7	±6
Pisa	±8	±8	±6
Dartmouth	±6	±7	±5
Adopted intrinsic age spreads	±7	±7	±6

Age spreads were estimated comparing observed luminosity spreads to simulated populations with a given intrinsic age spread, taking into account multiplicity, spots and observational uncertainties. Adopted median ages are listed in Table 11.

matches the simulated luminosity spreads for each Sco–Cen subgroup. We adopted the median subgroup ages listed in Table 11 as the mean age of our simulated populations to compare the luminosity spreads in our simulations to those from our observations. We adopt 1σ Gaussian age spreads of ±7 Myr, ±7 Myr and ±6 Myr for US, UCL and LCC, respectively. A plot showing the best matches to the observed luminosity spreads is shown in Fig. 7. Our results are summarized in Table 12. These age spreads indicate that 68 per cent of star formation in each subgroup occurred over a period of ∼14 Myr for US and UCL, and over a period of ∼12 Myr for LCC.

4.8 Spatial variation of ages

Blaauw (1964) divided Sco–Cen into the subgroups Upper Scorpius, Upper Centaurus-Lupus and Lower Centaurus Crux. However, Rizzuto et al. (2011) notes that, based on their updated membership study of Sco–Cen, the distribution of probable members indicates that the subgroups cannot be defined in a non-arbitrary manner. US has consistently been shown to be younger than the other two subgroups, and UCL and LCC have typically been assigned similar ages (Mamajek et al. 2002; Preibisch & Mamajek 2008; Pecaut et al. 2012). Given the large spatial extent of UCL and LCC, however, it is too simplistic to place them into two groups, each characterized by a single mean age. For example, the ∼50 pc size of LCC and adopted mean age of ∼17 Myr leads to an expected individual age uncertainty of ∼50 per cent, or ∼8 Myr, based on a star formation time-scale-size relation (see discussion in Soderblom et al. 2014). Here we attempt to examine the age structure of the entire association to discern if we see evidence for spatial substructure based on systematic differences in age as a function of position on the sky.

One possible method to investigate spatial variations of ages would be to simply evaluate the age of each member against pre-MS evolutionary tracks and spatially average their ages to create an age map. However, given the strong mass-dependent age trend we find with all the evolutionary tracks, this would tend to show regions with large numbers of low-mass stars as younger regions, when in fact this may be a systematic effect due to the evolutionary tracks. Therefore we do not use this method.

Systematically younger regions will tend to be more luminous than the mean association luminosity as a function of $T_{\rm eff}$. This is comparison does not depend on *any* theoretical models. To probe for statistically significant spatial variations of ages, *independent* of any evolutionary tracks, we look for concentrations of stars which lie above or below the average luminosity as a function of $T_{\rm eff}$. We use all the pre-MS members which have been studied spectroscopically. We place all stars from all three subgroups together on the H–R diagram and construct an empirical isochrone for the entire

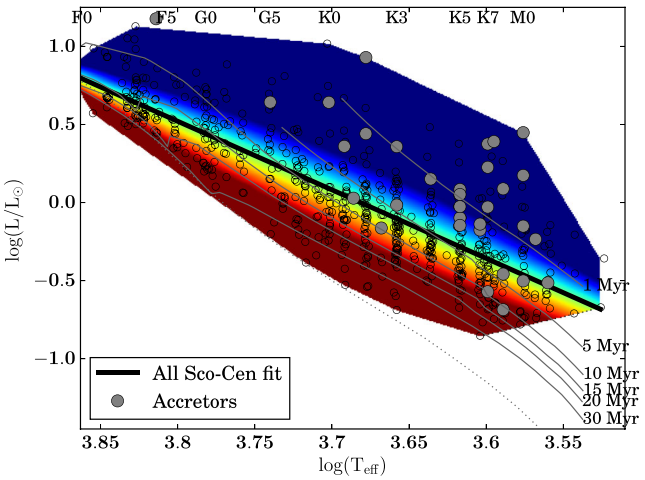

Figure 8. Empirical isochrone for 657 F/G/K-type members of all subgroups of Sco–Cen. We fit a line to create the empirical isochrone. We use individual stars' offsets above or below this empirical isochrone to create a relative age map, shown in Fig. 9. The coloured regions shown here correspond to the ages on the map in Fig. 9.

association, by fitting a line to $\log(L/\mathrm{L}_\odot)$ as a function of $T_{\rm eff}$. This is plotted in Fig. 8. Each star lies on the H–R diagram above or below this empirical isochrone. For each star we calculate this offset in units of the luminosity spread σ above or below the linear fit:

$$\mathrm{offset} = (\log(L/\mathrm{L}_\odot) - \langle\log(L/\mathrm{L}_\odot)\rangle)/\sigma_{\log(L/\mathrm{L}_\odot)}$$

We then spatially average their *offset*, above or below the empirical isochrone, in galactic coordinates, shown in Fig. 9. Regions on the sky with stars which are systematically more luminous than the average of the association will lie systematically above the empirical isochrone and will appear on the age map as younger. Likewise, stars in older regions will tend to be less luminous on average than the average of the association. In Fig. 9, we plot a spatial intensity map of the median offset from the empirical isochrone. The colored regions in Fig. 9 correspond to the same colored regions above or below the empirical isochrone in Fig. 8. Spatially averaging their offset from the empirical isochrone allows us to determine which regions have concentrations of systematically younger or older stars, relative to the age of the entire association, and independent of any theoretical models. This method avoids biases due to any mass-dependent age trends, and can identify younger or older regions without reference to any evolutionary tracks. The median distance of the F- and G-type stars is within ∼4 pc of the median distance of the K-type stars in each subgroup, and is not systematically biased nearer or farther. Furthermore, the variable extinction across the association ranges from ∼0.0−0.5 mag (25–75 per cent interquartile range), which would not significantly bias the spatial distribution of ages. Thus it is likely that our selection methods do not exhibit any systematic spatial biases for younger or older ages across the association that would bias the age map.

We wish to assign mean isochronal ages of these regions using evolutionary models. In order to assign ages to the regions shown on the map, we use the F5 through G9 stars to anchor the regions to an age. For example, the F5 through G9 stars that lie 0.33σ to 0.66σ *below* the median isochrone, irrespective of their location in the association, have a median age of 18 Myr. Therefore, any

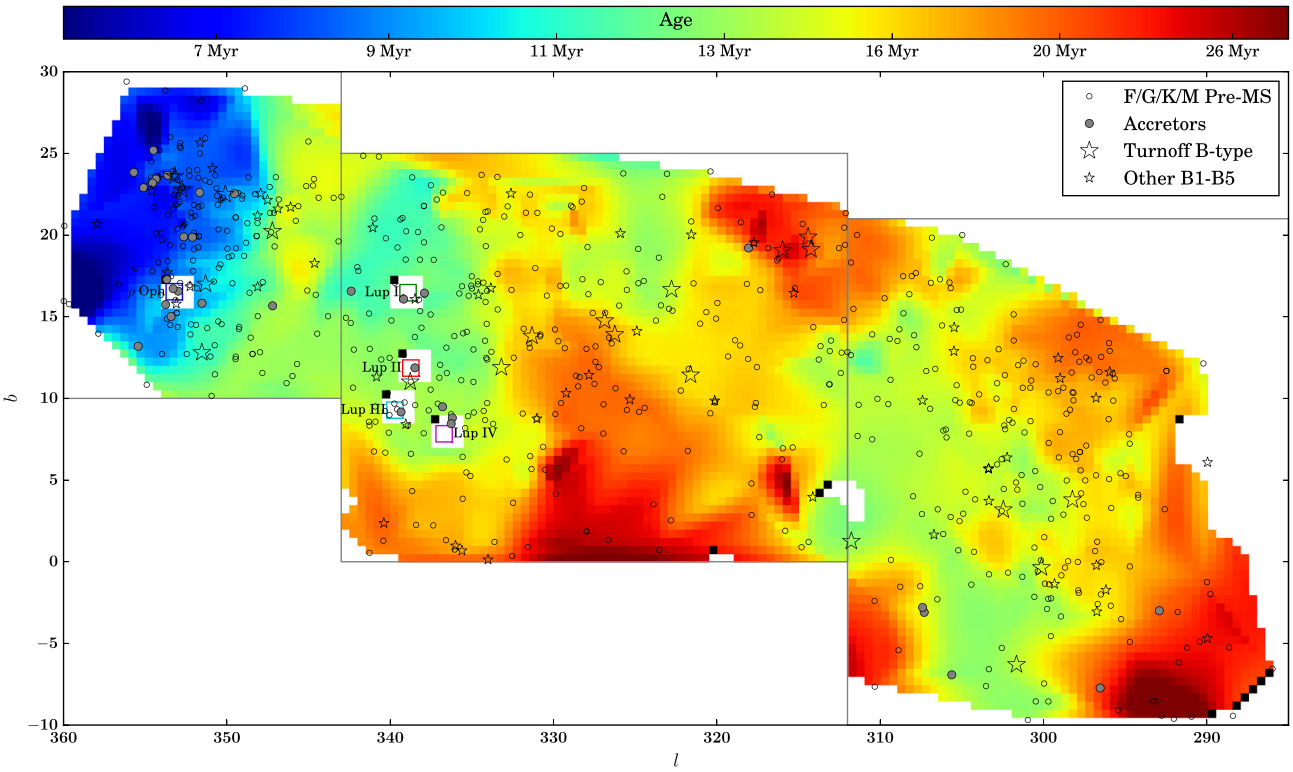

Figure 9. Spatial distribution of 657 F/G/K/M-type pre-MS members (solid dots) with spatially averaged median ages plotted on an 'age map'. The map is created by evaluating the median luminosity offset relative to the spread in luminosity $(\log(L/\mathrm{L}_\odot) - \langle\log(L/\mathrm{L}_\odot)\rangle)/\sigma_{\log(L/\mathrm{L}_\odot)}$ of stars in a 5° radius each (l, b). These offsets are then correlated with ages using the F5 through G9 stars that fall in those offset bins. We have masked the age map over regions cospatial with the Ophiuchus and Lupus clouds.

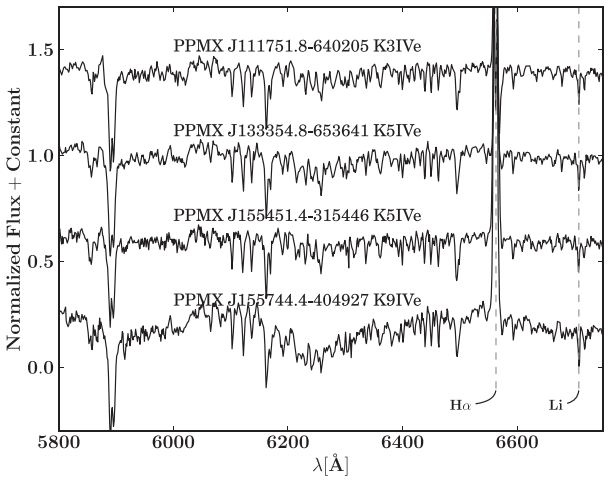

Figure 10. Representative spectra of new Sco–Cen members with strong Hα emission consistent with accretion.

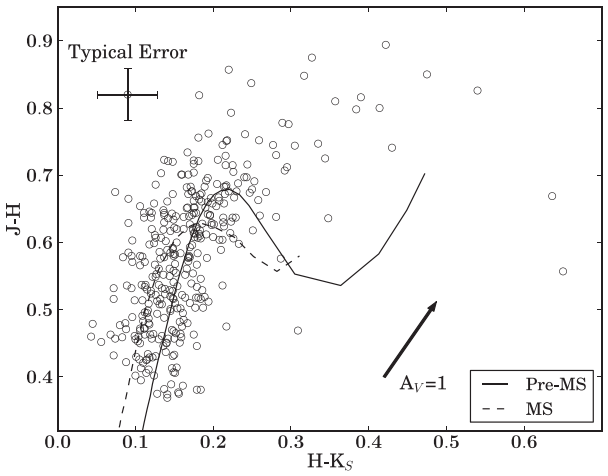

Figure 11. H–K_S versus J–H colours for new candidate Sco–Cen members. The dwarf and pre-MS stellar locus from Pecaut & Mamajek (2013) are included shown as the dashed and solid lines, respectively.

region with a median offset of 0.33σ to 0.66σ below the empirical isochrone is assigned an age of ∼18 Myr. The age map makes use of 657 F-M pre-MS stars to establish *relative* ages from the mean Sco–Cen empirical isochrone, but the ages are adopted from the F5-G9 stars. We discuss our motivations for adopting the F- and G-type ages in Section 5.1.

4.9 Circumstellar discs

4.9.1 Spectroscopic accretion disc fraction

Giant planet formation is fundamentally limited by the lifetimes of gas-rich protoplanetary discs surrounding the host star (Pollack et al. 1996). The gas disc dissipation time-scale therefore provides an upper limit to the giant planet formation time-scale. Differences in disc dissipation time-scales for stars in different mass bins can provides critical data for inferring how the planet formation process differs around stars of various masses. Additionally, a census for gas-rich circumstellar discs allows for follow-up studies of the gas disc itself (e.g. Zhang et al. 2013) or the star–disc interaction (e.g. Bouvier et al. 2007; Nguyen et al. 2009).

Here we perform a census of accretion discs for our sample using Hα emission as an accretion diagnostic. Various criterion have been proposed using Hα as an accretion indicator, and we adopt the spectral type dependent empirical criterion of Barrado y Navascués & Martín (2003). If our measured or adopted EW(Hα) (see Table 7) exceeds the Barrado y Navascués & Martín (2003) criterion, we count the object as an accretor. Our accretion disc fraction excludes the 28 Sco–Cen members in our sample which lack Hα measurements. Sample spectra for Sco–Cen members with Hα in emission consistent with accretion are shown in Fig. 10.

Using the Barrado y Navascués & Martín (2003) criteria, we identified 10/108 accretors in US, or a spectroscopic accretion disc fraction of $9.3^{+3.6}_{-2.1}$ per cent. In UCL and LCC we have 5/154 and 4/127 accretors, or spectroscopic accretion disc fractions of $3.2^{+2.1}_{-0.9}$ per cent and $3.1^{+2.4}_{-0.9}$ per cent, respectively. These disc fractions include all K and M-type members in our sample with EW(Hα) measurements, and therefore have masses predominantly ∼0.7–1.3 $M_\odot$, with a few M-type stars as low as ∼0.5 $M_\odot$; for statistics on the K-type members *only*, refer to Table 13.

4.9.2 Infrared excess disc fraction

Infrared photometry can be used to identify the presence of circumstellar matter with different wavelengths used to probe matter at different temperatures. To probe cooler, dusty debris around young stars, 20μm and longer wavelengths are useful. We examine Sco–Cen members for excesses in H–K_S, K_S–$W1$, K_S–$W2$, K_S–$W3$, and K_S–$W4$ colours, shown in Figs 11, 12 and 13, in order to identify Sco–Cen members exhibiting IR excesses which may indicate the presence of a disc and allow us to infer its evolutionary state. These stars are also plotted against Hα equivalent width (EW(Hα)) in Fig. 14, demonstrating that accreting stars identified with the Barrado y Navascués & Martín (2003) EW(Hα) criteria also typically exhibit a $W1$ band excess due to the presence of a warm circumstellar gas disc. We identify stars above the 3σ dispersion in the young stellar locus, as defined in Pecaut & Mamajek (2013), as having an excess in that band. We use 3σ as a conservative criterion, to avoid reporting excesses with a small confidence level. To avoid reporting false excesses due to scatter in the photometry, we only report an infrared excess if that object is also above the 3σ dispersion in the young stellar locus for that band *and* all bands at longer wavelengths.

Discs in young populations such as Sco–Cen may be found in a variety of stages of evolution. Here we attempt to classify the discs into the disc classification scheme described by Espaillat et al. (2012), using the observational criteria described by Luhman & Mamajek (2012). Based on the boundary between the full discs and transitional, evolved and debris discs for the stars classified in Luhman & Mamajek (2012), we identify 'full discs' as those with E(K_S–$W3$) > 1.5 and E(K_S–$W4$) > 3.2, 'transitional discs' as those with E(K_S–$W4$) > 3.2 but have E(K_S–$W3$) < 1.5. We then identify 'evolved discs' as those with E(K_S–$W4$) > 3.2 and E(K_S–$W3$) > 0.5 and 'debris discs' as those with E(K_S–$W4$) < 3.2 and E(K_S–$W3$) < 0.5. Colour excesses and classifications are shown in Fig. 15. Four stars had excesses in $W1$, $W2$ or $W3$ but no reliable $W4$. We classify them as evolved or debris discs based on their lack of spectroscopic signatures of accretion and their E(K_S–$W2$) and E(K_S–$W3$).

Discs classified using this method are listed in Table 7. Our sample contains a small number of G- and M-type members of Sco–Cen. Therefore, in Table 13 we summarize infrared excess

Table 13. Infrared excess and spectroscopic accretion disc fractions for K-type (∼0.7–1.3 $M_\odot$) members in Sco–Cen.

Band/Criteria/Disc type	US	UCL	LCC
EW(Hα)	6/84 ($7.1^{+3.9}_{-1.9}$ per cent)	5/145 ($3.4^{+2.2}_{-1.0}$ per cent)	4/119 ($3.4^{+2.5}_{-1.0}$ per cent)
K_S	6/89 ($6.7^{+3.7}_{-1.8}$ per cent)	6/158 ($3.8^{+2.2}_{-1.0}$ per cent)	2/119 ($1.7^{+2.1}_{-0.5}$ per cent)
*W*1	11/89 ($12.4^{+4.3}_{-2.7}$ per cent)	9/157 ($5.7^{+2.4}_{-1.3}$ per cent)	4/119 ($3.4^{+2.5}_{-1.0}$ per cent)
*W*2	14/89 ($15.7^{+4.6}_{-3.1}$ per cent)	9/157 ($5.7^{+2.4}_{-1.3}$ per cent)	4/119 ($3.4^{+2.5}_{-1.0}$ per cent)
*W*3	24/89 ($27.0^{+5.2}_{-4.1}$ per cent)	17/157 ($10.8^{+3.0}_{-2.0}$ per cent)	8/118 ($6.8^{+3.1}_{-1.6}$ per cent)
*W*4	25/36 ($69.4^{+6.5}_{-8.5}$ per cent)	33/72 ($45.8^{+5.9}_{-5.6}$ per cent)	8/86 ($9.3^{+4.1}_{-2.2}$ per cent)
Full	8/89 ($9.0^{+4.0}_{-2.2}$ per cent)	8/157 ($5.1^{+2.4}_{-1.2}$ per cent)	4/118 ($3.4^{+2.5}_{-1.0}$ per cent)
Transitional	2/89 ($2.2^{+2.8}_{-0.7}$ per cent)	0/157 (<2.3 per cent; 95 per cent C.L.)	0/118 (<3.0 per cent; 95 per cent C.L.)
Evolved	2/89 ($2.2^{+2.8}_{-0.7}$ per cent)	1/157 ($0.6^{+1.4}_{-0.2}$ per cent)	0/118 (<3.0 per cent; 95 per cent C.L.)

Spectroscopic accretion and IR excess fractions shown above for K-type members of Sco–Cen only, with masses ∼0.7–1.3 $M_\odot$.

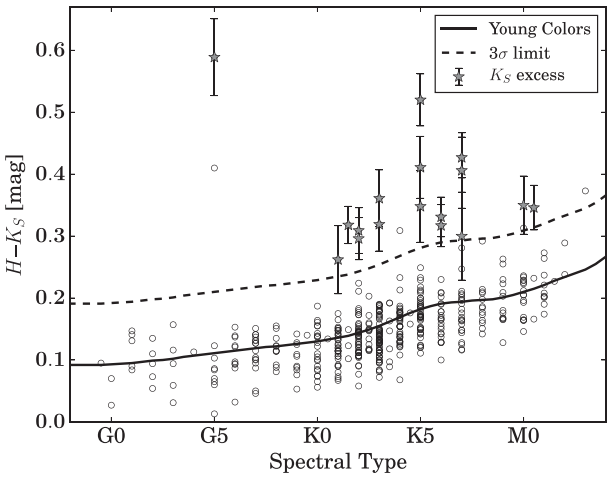

Figure 12. Spectral type versus dereddened H–K_S colour for Sco–Cen members. The solid line is the pre-MS photospheric colours from Pecaut & Mamajek (2013). The dashed line is the 3σ dispersion in the photospheric colours. Members with colour excesses above the 3σ dispersion in the photospheric colours in this and all bands at longer wavelength are identified as having a K_S band excess (gray stars).

fractions for only K-type (∼0.7–1.3 $M_\odot$) Sco–Cen members in the 2MASS K_S band and the four *WISE* bands.

5 DISCUSSION

5.1 Which ages are reliable?

Depending on which isochronal ages we examine, we obtain different mean subgroup ages. However, given the $T_{\rm eff}$-dependent age trend present in Fig. 5, we see several reasons to distrust ages from M-type stars. The most obvious reason is that evolutionary models have difficulty predicting the radii of main-sequence M-type stars, systematically underestimating their radii by ∼5–20 per cent (Torres & Ribas 2002; Boyajian et al. 2012; see also Kraus et al. 2011). Hillenbrand & White (2004) have compared dynamically constrained masses with predictions from pre-MS evolutionary models and found that the models systematically underpredict the masses of stars 5–20 per cent for masses under 0.5 $M_\odot$. On the other hand, they found that for masses above 1.2 $M_\odot$, dynamical masses and predicted masses from all models are consistent. As stated in Hillenbrand et al. (2008), the likely source for the poor performance of models in the low-mass regime is incomplete knowledge of opacity sources and the difficulty in modelling convection. One of the large sources of uncertainty particularly applicable to modelling low-mass stars is the role magnetic fields play in convection, as discussed in Feiden (2016). Strong magnetic fields can give rise to large star spots on the surface of the star, which will may cause the star to exhibit more than one surface temperature (Stauffer et al. 2003). Somers & Pinsonneault (2015) have studied the effect of star spots on inferred ages and masses in pre-main-sequence stars, and find that spots will tend to inflate the radii of young stars and shift them to a cooler $T_{\rm eff}$. The effect is that spots will make older stars appear to be younger and less massive than implied by the evolutionary models. Somers & Pinsonneault (2015) offer age and mass correction factors which can be used to estimate less biased, more accurate masses and ages from published evolutionary tracks. Given the problems with radii and mass discrepancies from models as well as the potential influence of spots, and that there are higher-mass F- and G-type isochronal ages available, it is preferable to avoid the adopting ages from the K- and M-type members.

What about kinematic ages? Kinematic 'expansion' or 'traceback' ages are not dependent on stellar interior models and therefore offer the prospect of nearly model-free ages. Song et al. (2012) argues that kinematic expansion ages can function as model-independent age benchmarks which can then be used to establish a model-independent age scale. Age indicators such as Li can then be used to establish relative ages among different stellar populations. This is an interesting idea in principle, however there are a few major issues with kinematic traceback ages.

One major problem is that one must assume that the association was in a physically smaller configuration at some time in the past. The data presented in Section 4.8 indicates substantial substructure in Sco–Cen. This is consistent with work in other OB associations, for example, Cygnus OB2 also exhibits substantial substructure (Wright et al. 2014, 2016), and was never a compact, bound cluster. The presences of substantial substructure invalidates the assumption that the members of these associations were in more compact configurations in the past, which prevents the determination of a meaningful kinematic age.

Another major issue is that the results from kinematic ages are very sensitive to the implementation. A recent example is that in the TW Hydra Association (TWA). A commonly quoted age for TWA is 8 Myr based on the kinematic traceback of de la Reza, Jilinski & Ortega (2006). However, their kinematic traceback was based on a sample of only four stars, which was contaminated by TWA 19, a member of LCC (Mamajek et al. 2002). Mamajek (2005) calculated a kinematic expansion age for TWA using kinematic parallaxes and

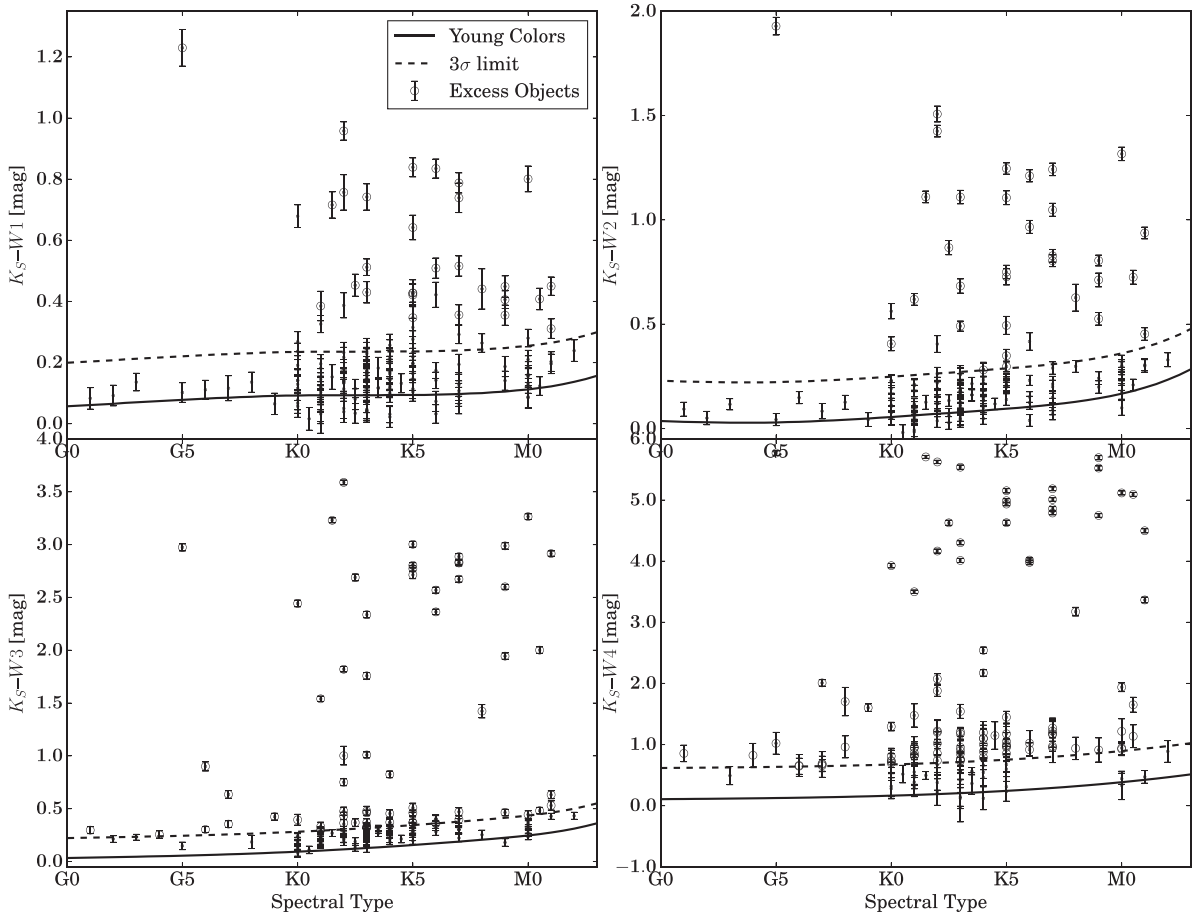

Figure 13. Spectral type versus infrared colours K_S–$W1$, K_S–$W2$, K_S–$W3$, and K_S–$W4$ for Sco–Cen members. The solid lines are the pre-MS photospheric colours from Pecaut & Mamajek (2013). Members with colour excesses above the 3σ dispersion of photospheric colours in that band and all bands at longer wavelength are identified as having excess emission from circumstellar discs. Objects with colour uncertainties greater than 0.25 mag are not shown.

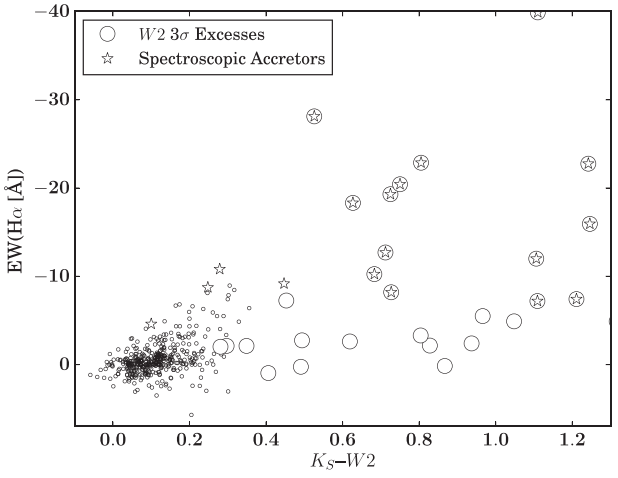

Figure 14. K_S–$W2$ colour versus EW(Hα) for Sco–Cen members. Members spectroscopically identified as accretors with the Barrado y Navascués & Martín (2003) criteria are shown as stars. Members exhibiting a K_S–$W2$ colour excess are shown as large circle.

a vetted list of members and obtained a lower limit of ∼10 Myr on the expansion age at 95 per cent confidence, though the data were only weakly consistent with expansion. More recently, Weinberger, Anglada-Escudé & Boss (2013) performed a kinematic traceback of TWA using a vetted list of members and trignometric parallaxes. The Weinberger et al. (2013) traceback result indicated the members were never in a significantly more compact configuration. Another TWA study, Ducourant et al. (2014), independently obtained trignometric parallaxes for 13 stars, identify 31 as a comoving association, 25 of which had radial velocity and trignometric parallax data. This study obtained a traceback age for TWA of 7.5 ± 0.7 Myr. However, this result was based on a sample of 16 stars with converging motions, obtained after removing 9 stars which systematically drifted from the centre of the association when traced back in time. Similarly, an often-quoted age for Upper Sco is the 5 Myr expansion age derived from proper motion data by Blaauw (1978). However, it was demonstrated by Brown, Dekker & de Zeeuw (1997), using simulations of expanding OB associations, that expansion ages inferred from proper motions alone all converged to ∼4 Myr, no matter the actual kinematic age. A recent examination of the expansion age in Upper Sco by Pecaut et al. (2012), using radial velocity data, gave a lower limit of ∼10 Myr at 95 per cent confidence, though the data were consistent with no expansion. Finally, we mention that the adopted kinematic expansion age of the β Pictoris moving group (BPMG) of 12 Myr, estimated by Song, Zuckerman & Bessell (2003), has been re-evaluated by Mamajek & Bell (2014). The Mamajek & Bell (2014) study found the modern BPMG kinematic data was only weakly indicitave of expansion, and that the age is only weakly constrained by the kinematic data, giving a 95 confidence limit of 13–58 Myr. We conclude that the there is

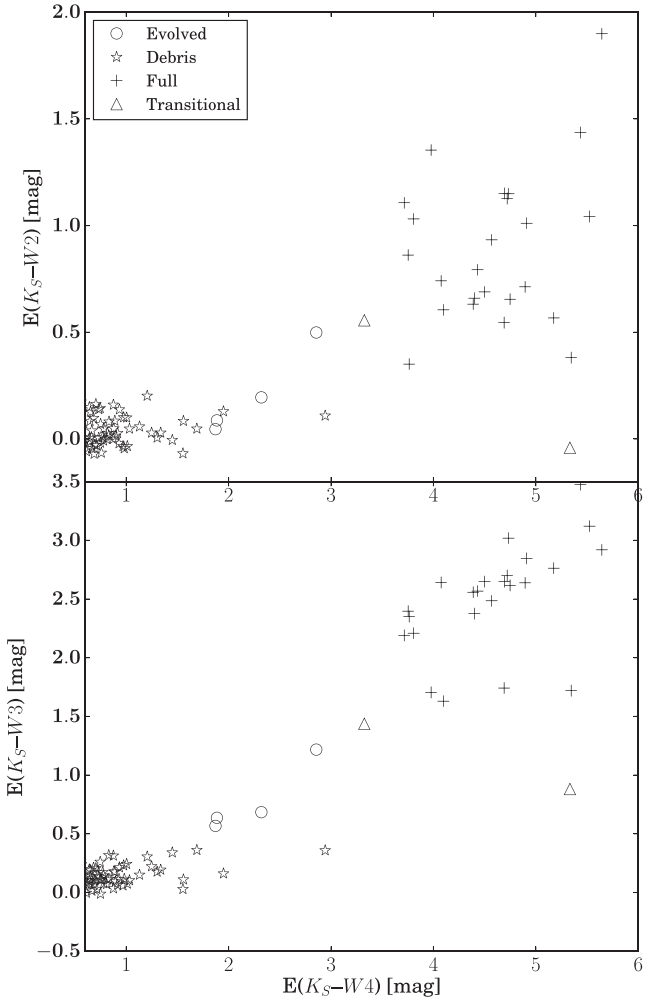

Figure 15. Color excesses above the photosphere for stars in Sco–Cen exhibiting an infrared excess.

no well-constrained kinematic traceback age for either Sco–Cen or the groups used to bracket its age (e.g. TWA, BPMG) that has withstood the scrutiny of improved data, and that they simply do not yield useful age constraints given the current precision of the available data.

Another relevant chronometric technique is the use of the lithium depletion boundary (LDB) to determine the age of a stellar population. By detecting the stellar $T_{\rm eff}$ or luminosity above which all the stars have exhibit Li depletion and comparing this with evolutionary model predictions, one can obtain an age which is independent of distance. LDB ages have been calculated for several of the nearby, young moving groups (Mentuch et al. 2008; Binks & Jeffries 2014) but the subgroups of Sco–Cen do not yet have a reliable LDB age. The results of Cargile, James & Jeffries (2010) suggests that lithium depletion boundary ages and modern nuclear main-sequence turn-off ages are in agreement when convective core overshooting is included in the models of high-mass stars (e.g. Ekström et al. 2012). However, LDB ages are typically much older than pre-MS contraction ages, and it has been suggested that this problem is related to the radii discrepancy in M-type stars (Yee & Jensen 2010; Somers & Pinsonneault 2015).

Recent discoveries of eclipsing binaries, particularly in Upper Scorpius using the data obtained using the Kepler K2 mission, should help evolutionary models significantly by providing well-constrained radii and masses at these young ages. Particularly, the recently published discoveries by David et al. (2016), Alonso et al. (2015), Lodieu et al. (2015), and Kraus et al. (2015), will add a signifcant number of benchmark eclipsing binaries with tightly constrained, nearly model-independent parameters for objects in Upper Scorpius. Masses and radii for the eclipsing binary UScoCTIO 5 from Kraus et al. (2015), when compared to the Baraffe et al. (2015) evolutionary models, already provide some concordance with the older ∼10 Myr ages from the F- and G-type stars, though more theoretical work remains to be completed.

5.2 How 'coeval' are the Sco–Cen subgroups?

Previous studies of Sco–Cen have attempted to quantify the observed age spread in the subgroups. In Upper Sco, Preibisch et al. (2002), adopting an age of 5 Myr, concluded that the age spread was $\lesssim$1–2 Myr. Their results account for the effects of binarity, a distance spread, and observational uncertainties. This is consistent with the results of Slesnick et al. (2006), who similarly constrained the age spread in the northern part of Upper Sco to be less than ±3 Myr (uniform distribution) using similar assumptions. In their study of UCL and LCC, Mamajek et al. (2002) have examined age spreads in the older subgroups and have constrained the star formation to have occurred over a time period of ±3 Myr and ±2 Myr (1σ) for UCL and LCC, respectively.

Our age spreads are larger than those previously reported, with 1σ age spreads of ±7 Myr, ±7 Myr, and ±6 Myr for US, UCL and LCC, respectively. Our age spread of ±7 Myr for Upper Sco is much larger than the age spreads detected by Preibisch et al. (2002) and Slesnick, Hillenbrand & Carpenter (2008). However, the age map in Fig. 9 indicates that there is an age gradient from the southeastern part of US to the north-west, with the northwestern part being younger. The Slesnick et al. (2008) and Preibisch et al. (2002) low-mass samples were drawn from smaller regions (∼150 deg^2 and ∼160 deg^2, respectively) than our sample in Upper Sco (drawn from the entire ∼320 deg^2), which could be responsible for the smaller detected age spreads. However, the likely reason our inferred age spreads in US are larger than previous results is that we adopt a mean age of 10 Myr, twice as old as the Slesnick et al. (2008) or Preibisch et al. (2002) studies. A given luminosity spread at a younger age corresponds to a smaller inferred dispersion in ages than the same luminosity spread at an older age, simply because the younger isochrones are spaced farther apart in luminosity than those at older ages.

Slesnick et al. (2008) suggests that spreads in H–R diagram positions may not be an accurate proxy for spreads in age. They demonstrate this by comparing two nearly identical spectra for members in US, with spectroscopic surface gravity indicators which are indicative of nearly identical surface gravity. However, their H–R diagram positions suggests their ages differ by more than 10 Myr! Jeffries et al. (2011) use constraints on the disc lifetime to show that the age spread in the Orion nebula Cluster must be less than 0.14 dex in log (Age), though the age spreads inferred from the H–R diagram show a 0.4 dex dispersion in log (Age). These results suggest that scatter in the H–R diagram may not be a reliable indicator of age spreads. However, the H–R diagram remains the best observational indicator available at the present time for revealing any intrinsic age spreads. See Soderblom et al. (2014) for a more detailed and complete discussion regarding age spreads.

As stated previously, our age map does indicate there is a clear age gradient in US as it merges into UCL. The southern part of LCC is also noticeably younger than other parts of LCC, confirming the

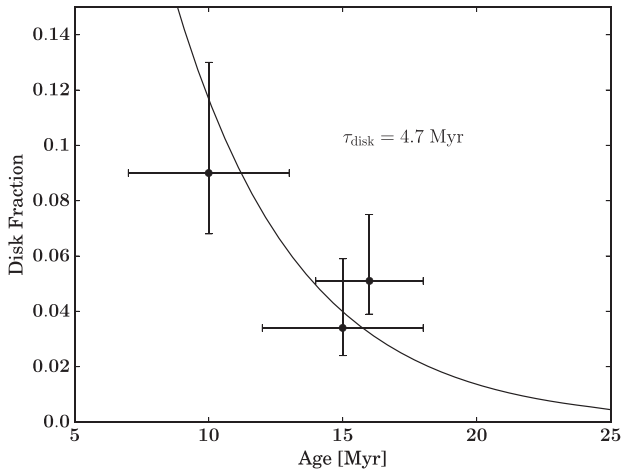

Figure 16. Mean subgroup age versus disc fraction ('Full Disc'; see Table 13) for K-type stars, ∼0.7–1.3 $M_{\odot}$, from the three subgroups of Sco–Cen. The best-fitting exponential decay curvey $f_{\rm disc} = e^{-t/\tau_{\rm disc}}$ has $\tau_{\rm disc}$=4.7 Myr.

suggestion first raised in Preibisch & Mamajek (2008). We note that there are no main-sequence turn-off stars in northern LCC, which, considering the younger age of southern LCC, accounts for the turn-off age of LCC being much younger than UCL. The star formation history of Sco–Cen, as inferred from the H–R diagram positions, appears to be more complex than previously treated. The spatial distribution of ages is suggestive that the current division of three distinct, coeval subgroups is overly simplistic and a separation into smaller units may be warranted. We avoid speculating further on scenarios of triggered star formation here, leaving that discussion to a future study.

5.3 Circumstellar disc census

Observations of young clusters and associations of ages from ∼1 to >100 Myr have given strong indication that the protoplanetary disc dispersal time-scale is very short, with an e-folding time of ∼2.5 Myr (Mamajek 2009; Fedele et al. 2010). This is qualitatively consistent with what we seen in Sco–Cen: 9 per cent of Upper Sco K-type stars host an optically thick protoplanetary disc ('Full Disc' in the Espaillat et al. 2012 nomenclature) at an age of ∼10 Myr, whereas ≃4 per cent of the K-type stars in the older subgroups UCL and LCC host a full disc (Table 13). However, the e-folding time of 2.5 Myr was estimated adopting an Upper Sco age of 5 Myr, along with many other young clusters. Naylor (2009) has argued that pre-MS ages systematically underestimate cluster ages, and that ages based on high-mass stars, typically double the ages estimated from the low-mass stars, are more likely to be correct (Bell et al. 2013). Using the ages we adopt for the Sco–Cen subgroups, what disc dispersal time-scale does this imply? We plot the primordial disc fractions ('Full Disc' from Table 13) as a function of age in Fig. 16 and, following Mamajek (2009), fit an exponential decay curve to the data ($f_{\rm disc} = {\rm e}^{-t/\tau_{\rm disc}}$). We obtain a mean protoplanetary disc e-folding time-scale of 4.7 Myr for K-type stars (∼0.7–1.3 $M_{\odot}$). This is ∼2 Myr longer than the time-scale estimated in Mamajek (2009), and would imply a longer time-scale available for planet formation, but consistent with the findings of Bell et al. (2013).

Finally, we note that our K-type disc fraction is larger than what is observed for the higher mass-stars in the same subgroups (Mamajek et al. 2002; Carpenter et al. 2009; Luhman & Mamajek 2012; Pecaut et al. 2012). This is consistent with the mass-dependent trend first identified by Carpenter et al. (2006) and further confirmed by Luhman & Mamajek (2012) in Upper Sco, as well as the results of Hernández et al. (2007) from the younger σ Ori association at ∼6 Myr (Bell et al. 2013). Ribas, Bouy & Merín (2015) have summarized these mass-dependent disc fraction trends using the nearby young stellar associations within ∼500 pc, and have come to a similar conclusion – that the disc dispersal time depends on stellar mass, with the low-mass stars retaining their discs longer. For Sco–Cen, however, we still have very poor statistics for M-type stars in the older subgroups, which highlights the need for future surveys to push the membership census to cooler spectral types in UCL and LCC (e.g. Murphy et al. 2015).

6 CONCLUSIONS

We can summarize the findings from our survey as follows.

(i) We have performed a survey for new, low-mass K- and M-type members of all three subgroups of Sco–Cen. Using Li, X-ray, and proper motion data, we identify 156 new pre-MS members of Sco–Cen.

(ii) Using our newly identified members together with previously known members of Sco–Cen, we utilize Hα as an accretion diagnostic and identify stars with Hα emission levels consistent with accretion. We estimate a spectroscopic accretion disc fraction of $7.1^{+3.9}_{-1.9}$ per cent, $3.4^{+2.2}_{-1.0}$ per cent and $3.4^{+2.5}_{-1.0}$ per cent for solar analog pre-MS K-type stars (∼0.7–1.3 $M_{\odot}$) in US, UCL and LCC, respectively, consistent with a protoplanetary disc decay e-folding time-scale of ∼4.7 Myr, or half-life of ∼3.3 Myr.

(iii) Similar to previous results in other star-forming regions (e.g. Hillenbrand 1997; Hillenbrand et al. 2008; Bell et al. 2013), we observe a $T_{\rm eff}$-dependent age trend in all three subgroups of Sco–Cen, for all sets of evolutionary tracks.

(iv) We adopt median ages of 10 ± 3 Myr, 16 ± 2 Myr and 15 ± 3 Myr for US, UCL and LCC, respectively, when considering the revised nuclear ages as well as the pre-MS contraction ages from the F- and G-type stars.

(v) We obtain estimates for the intrinsic age spread in each subgroup through a grid of Monte Carlo simulations which take into account binarity, spots, and observational uncertainties. Assuming the median ages obtained above, and modelling the age distribution as a Gaussian, we find that 68 per cent of the star formation in US, UCL, and LCC occured over time-scales of ±7 Myr, ±7 Myr, and ±6 Myr, respectively. Thus when adopting an age of ∼10 Myr for Upper Sco, we detect an intrinsic age spread of ±7 Myr (1σ).

(vi) Using members from our X-ray sample as well as F- and G-type members of Sco–Cen, we create an age map of the Sco–Cen complex. We find that the star formation histories of the UCL and LCC, the older subgroups, are indicative of substructure and are not consistent with a simple triggered star formation scenario. The groups are not each monolithic episodes of star formation, but likely an ensemble of small subgroups, exhibiting significant substructure.

ACKNOWLEDGEMENTS

We would like to thank the anonymous referee, whose comments and suggestions improved the quality of this work. This work has been supported by funds from the School of Arts and Sciences

at the University of Rochester and NSF grants AST-1008908 and AST-1313029. EEM acknowledges support from the NASA Nexus for Exoplanet System Science programme (NExSS). We thank Fred Walter for the use of his SMARTS RC-spectrograph pipeline for reducing the data obtained at the SMARTS 1.5 m telescope at Cerro Tololo, Chile, as well as Jose Velasquez and Manuel Hernandez for their help and advice at the telescope. This research was made possible through the use of the AAVSO Photometric All-Sky Survey (APASS), funded by the Robert Martin Ayers Sciences Fund. This publication makes use of data products from the Two Micron All Sky Survey, which is a joint project of the University of Massachusetts and the Infrared Processing and Analysis Center/California Institute of Technology, funded by the National Aeronautics and Space Administration and the National Science Foundation. This publication makes use of data products from the *Wide-field Infrared Survey Explorer*, which is a joint project of the University of California, Los Angeles, and the Jet Propulsion Laboratory/California Institute of Technology, funded by the National Aeronautics and Space Administration.

REFERENCES

Allard F., Homeier D., Freytag B., 2012, Phil. Trans. R. Soc. A, 370, 2765
Alonso R., Deeg H. J., Hoyer S., Lodieu N., Palle E., Sanchis-Ojeda R., 2015, A&A, 584, L8
Ardila D., Martín E., Basri G., 2000, AJ, 120, 479
Asplund M., Grevesse N., Sauval A. J., 2005, in Barnes T. G., III, Bash F. N., eds, ASP Conf. Ser. Vol. 336, Cosmic Abundances as Records of Stellar Evolution and Nucleosynthesis. Astron. Soc. Pac., San Francisco, p. 25
Balona L. A., 1994, MNRAS, 268, 119
Baraffe I., Homeier D., Allard F., Chabrier G., 2015, A&A, 577, A42
Barrado y Navascués D., Martín E. L., 2003, AJ, 126, 2997
Bell C. P. M., Naylor T., Mayne N. J., Jeffries R. D., Littlefair S. P., 2012, MNRAS, 424, 3178
Bell C. P. M., Naylor T., Mayne N. J., Jeffries R. D., Littlefair S. P., 2013, MNRAS, 434, 806
Bell C. P. M., Rees J. M., Naylor T., Mayne N. J., Jeffries R. D., Mamajek E. E., Rowe J., 2014, MNRAS, 445, 3496
Binks A. S., Jeffries R. D., 2014, MNRAS, 438, L11
Blaauw A., 1946, Publ. Kapteyn Astron. Lab. Groningen, 52, 1
Blaauw A., 1964, ARA&A, 2, 213
Blaauw A., 1978, in Mirzoyan L. V., ed., Problems of Physics and Evolution of the Universe. Armenian Academy of Sciences, Yerevan, p. 101
Bodenheimer P., 1965, ApJ, 142, 451
Bouvier J., Appenzeller I., 1992, A&AS, 92, 481
Bouvier J., Alencar S. H. P., Harries T. J., Johns-Krull C. M., Romanova M. M., 2007, in Reipurth B., Jewitt D., Keil K., eds, Protostars and Planets V: Magnetospheric Accretion in Classical T Tauri Stars. Univ. Arizona Press, Tucson, p. 479
Boyajian T. S. et al., 2012, ApJ, 757, 112
Brandner W., Alcala J. M., Kunkel M., Moneti A., Zinnecker H., 1996, A&A, 307, 121
Briceño C., Preibisch T., Sherry W. H., Mamajek E. A., Mathieu R. D., Walter F. M., Zinnecker H., 2007, in Reipurth B., Jewitt D., Keil K., eds, Protostars and Planets V. Univ. Arizona Press, Tucson, p. 345
Brown A. G. A., Dekker G., de Zeeuw P. T., 1997, MNRAS, 285, 479
Caffau E., Ludwig H.-G., Steffen M., Ayres T. R., Bonifacio P., Cayrel R., Freytag B., Plez B., 2008, A&A, 488, 1031
Caffau E., Maiorca E., Bonifacio P., Faraggiana R., Steffen M., Ludwig H.-G., Kamp I., Busso M., 2009, A&A, 498, 877
Caffau E., Ludwig H.-G., Steffen M., Freytag B., Bonifacio P., 2011, Sol. Phys., 268, 255
Carballo R., Wesselius P. R., Whittet D. C. B., 1992, A&A, 262, 106
Cargile P. A., James D. J., Jeffries R. D., 2010, ApJ, 725, L111
Carpenter J. M., Mamajek E. E., Hillenbrand L. A., Meyer M. R., 2006, ApJ, 651, L49
Carpenter J. M., Mamajek E. E., Hillenbrand L. A., Meyer M. R., 2009, ApJ, 705, 1646
Chen C. H., Mamajek E. E., Bitner M. A., Pecaut M., Su K. Y. L., Weinberger A. J., 2011, ApJ, 738, 122
Chen Y., Girardi L., Bressan A., Marigo P., Barbieri M., Kong X., 2014, MNRAS, 444, 2525
Churchwell E. et al., 2009, PASP, 121, 213
Cutri R. M. et al., 2012a, VizieR Online Data Catalog, 2281, 0
Cutri R. M. et al., 2012b, VizieR Online Data Catalog, 2311, 0
Cutri R. M. et al., 2014, VizieR Online Data Catalog, 2328, 0
Dahm S. E., Slesnick C. L., White R. J., 2012, ApJ, 745, 56
David T. J., Hillenbrand L. A., Cody A. M., Carpenter J. M., Howard A. W., 2016, ApJ, 816, 21
de Bruijne J. H. J., 1999a, MNRAS, 306, 381
de Bruijne J. H. J., 1999b, MNRAS, 310, 585
de Geus E. J., de Zeeuw P. T., Lub J., 1989, A&A, 216, 44
de la Reza R., Jilinski E., Ortega V. G., 2006, AJ, 131, 2609
de Zeeuw P. T., Hoogerwerf R., de Bruijne J. H. J., Brown A. G. A., Blaauw A., 1999, AJ, 117, 354
Dobbie P. D., Lodieu N., Sharp R. G., 2010, MNRAS, 409, 1002
Dolidze M. V., Arakelyan M. A., 1959, Astron. Z., 36, 444
Dotter A., Chaboyer B., Jevremović D., Kostov V., Baron E., Ferguson J. W., 2008, ApJS, 178, 89
Downes R. A., Keyes C. D., 1988, AJ, 96, 777
Duchêne G., Kraus A., 2013, ARA&A, 51, 269
Ducourant C., Teixeira R., Galli P. A. B., Le Campion J. F., Krone-Martins A., Zuckerman B., Chauvin G., Song I., 2014, A&A, 563, A121
Ekström S. et al., 2012, A&A, 537, A146
ESA, 1997, ESA SP-1200, The Hipparcos and Tycho Catalogues. ESA, Noordwijk
Espaillat C. et al., 2012, ApJ, 747, 103
Fedele D., van den Ancker M. E., Henning T., Jayawardhana R., Oliveira J. M., 2010, A&A, 510, A72
Feiden G. A., 2016, in Kastner J. H., Stelzer B., Metchev S. A., eds, Proc. IAU Symp., 314, 79
Feigelson E. D., Lawson W. A., 1997, AJ, 113, 2130
Feigelson E. D., Montmerle T., 1999, ARA&A, 37, 363
Filin A. Y., Satyvoldiev V., 1975, Perem. Zvezdy, 20, 161
Finkenzeller U., Basri G., 1987, ApJ, 318, 823
Fiorucci M., Munari U., 2003, A&A, 401, 781
Garrison R. F., 1967, ApJ, 147, 1003
Gray R. O., Garrison R. F., 1989, ApJS, 69, 301
Gray R. O., Napier M. G., Winkler L. I., 2001, AJ, 121, 2148
Gray R. O., Corbally C. J., Garrison R. F., McFadden M. T., Robinson P. E., 2003, AJ, 126, 2048
Gray R. O., Corbally C. J., Garrison R. F., McFadden M. T., Bubar E. J., McGahee C. E., O'Donoghue A. A., Knox E. R., 2006, AJ, 132, 161
Gregorio-Hetem J., Lepine J. R. D., Quast G. R., Torres C. A. O., de La Reza R., 1992, AJ, 103, 549
Grevesse N., Sauval A. J., 1998, Space Sci. Rev., 85, 161
Hauck B., Mermilliod M., 1998, A&AS, 129, 431
Henden A. A., Levine S. E., Terrell D., Smith T. C., Welch D., 2012, J. Am. Assoc. Var. Star Obs., 40, 430
Henize K. G., 1954, ApJ, 119, 459
Henize K. G., 1976, ApJS, 30, 491
Henry T. J., Walkowicz L. M., Barto T. C., Golimowski D. A., 2002, AJ, 123, 2002
Herbig G. H., Bell K. R., 1988, Lick Obs. Bull., No. 1111
Hernández J. et al., 2007, ApJ, 671, 1784
Hillenbrand L. A., 1997, AJ, 113, 1733
Hillenbrand L. A., White R. J., 2004, ApJ, 604, 741
Hillenbrand L. A., Bauermeister A., White R. J., 2008, in van Belle G., ed., ASP Conf. Ser. Vol. 384, 14th Cambridge Workshop on Cool Stars, Stellar Systems, and the Sun. Astron. Soc. Pac., San Francisco, p. 200
Hiltner W. A., Garrison R. F., Schild R. E., 1969, ApJ, 157, 313
Hoogerwerf R., de Bruijne J. H. J., de Zeeuw P. T., 2000, ApJ, 544, L133
Hou A., Parker L. C., Harris W. E., Wilman D. J., 2009, ApJ, 702, 1199

Houk N., 1978, Distributed by University Microfilms International, QB6.H, 77. Dept. Astronomy, Univ. Michigan, Ann Arbor
Houk N., 1982, Michigan Spectral Survey, Vol. 3. Dept. Astronomy, Univ. Michigan, Ann Arbor
Houk N., Smith-Moore M., 1988, Michigan Spectral Survey, Vol. 4. Dept. Astronomy, Univ. Michigan, Ann Arbor
Hughes J., Hartigan P., Krautter J., Kelemen J., 1994, AJ, 108, 1071
Høg E. et al., 2000, A&A, 355, L27
Ichikawa T., Nishida M., 1989, AJ, 97, 1074
Ishihara D. et al., 2010, A&A, 514, A1
Jeffries R. D., Littlefair S. P., Naylor T., Mayne N. J., 2011, MNRAS, 418, 1948
Johnson H. L., Morgan W. W., 1953, ApJ, 117, 313
Jones B. F., Fischer D. A., Stauffer J. R., 1996, AJ, 112, 1562
Kalas P. G. et al., 2015, ApJ, 814, 32
Keenan P. C., McNeil R. C., 1989, ApJS, 71, 245
Kirkpatrick J. D., Henry T. J., McCarthy D. W., Jr, 1991, ApJS, 77, 417
Kiss L. L. et al., 2011, MNRAS, 411, 117
Köhler R., Kunkel M., Leinert C., Zinnecker H., 2000, A&A, 356, 541
Kordopatis G. et al., 2013, AJ, 146, 134
Kraus A. L., Ireland M. J., 2012, ApJ, 745, 5
Kraus A. L., Tucker R. A., Thompson M. I., Craine E. R., Hillenbrand L. A., 2011, ApJ, 728, 48
Kraus A. L., Cody A. M., Covey K. R., Rizzuto A. C., Mann A. W., Ireland M. J., 2015, ApJ, 807, 3
Krautter J., Wichmann R., Schmitt J. H. M. M., Alcala J. M., Neuhauser R., Terranegra L., 1997, A&AS, 123, 329
Kroupa P., 2001, MNRAS, 322, 231
Lawson W. A., Lyo A.-R., Bessell M. S., 2009, MNRAS, 400, L29
Lodieu N. et al., 2015, A&A, 584A, 128
Luhman K. L., Mamajek E. E., 2012, ApJ, 758, 31
Mamajek E. E., 2005, ApJ, 634, 1385
Mamajek E. E., 2009, AIP Conf. Ser., 1158, 3
Mamajek E. E., 2013, Am. Astron. Soc. Meeting Abstr., 221, 331.06
Mamajek E. E., Bell C. P. M., 2014, MNRAS, 445, 2169
Mamajek E. E., Meyer M. R., Liebert J., 2002, AJ, 124, 1670
Mamajek E. E., Meyer M. R., Liebert J., 2006, AJ, 131, 2360
Mamajek E. E., Quillen A. C., Pecaut M. J., Moolekamp F., Scott E. L., Kenworthy M. A., Collier Cameron A., Parley N. R., 2012, AJ, 143, 72
Mamajek E. E., Pecaut M. J., Nguyen D. C., Bubar E. J., 2013, Protostars and Planets VI, Poster #1K086. Heidelberg
Martin E. L., Montmerle T., Gregorio-Hetem J., Casanova S., 1998, MNRAS, 300, 733
Mason B. D., Wycoff G. L., Hartkopf W. I., Douglass G. G., Worley C. E., 2001, AJ, 122, 3466
Mathieu R. D., Walter F. M., Myers P. C., 1989, AJ, 98, 987
Mentuch E., Brandeker A., van Kerkwijk M. H., Jayawardhana R., Hauschildt P. H., 2008, ApJ, 689, 1127
Mermilliod J.-C., Mermilliod M., 1994, Catalogue of Mean UBV Data on Stars, VI. Springer-Verlag, Berlin, Heidelberg, New York
Morgan W. W., Keenan P. C., 1973, ARA&A, 11, 29
Morgan W. W., Abt H. A., Tapscott J. W., 1978, Revised MK Spectral Atlas for Stars Earlier than the Sun. Yerkes Observatory, Williams Bay and Kitt Peak National Observatory, Tucson
Müller A., Carmona A., van den Ancker M. E., van Boekel R., Henning T., Launhardt R., 2011, A&A, 535, L3
Murphy S. J., Lawson W. A., Bento J., 2015, MNRAS, 453, 2220
Napiwotzki R., Schoenberner D., Wenske V., 1993, A&A, 268, 653
Naylor T., 2009, MNRAS, 399, 432
Nguyen D. C., Jayawardhana R., van Kerkwijk M. H., Brandeker A., Scholz A., Damjanov I., 2009, ApJ, 695, 1648
Nguyen D. C., Mamajek E., Pecaut M., 2013, Protostars and Planets VI. Poster #1G024, Heidelberg
Nieva M.-F., 2013, A&A, 550, A26
Park S., Finley J. P., 1996, AJ, 112, 693
Pecaut M. J., Mamajek E. E., 2013, ApJS, 208, 9
Pecaut M. J., Mamajek E. E., Bubar E. J., 2012, ApJ, 746, 154
Petrov P. P., Satyvoldiev V., 1975, Perem. Zvezdy Prilozhenie, 2, 221
Pollack J. B., Hubickyj O., Bodenheimer P., Lissauer J. J., Podolak M., Greenzweig Y., 1996, Icarus, 124, 62
Preibisch T., Mamajek E., 2008, Reipurth B. ed., The Nearest OB Association: Scorpius–Centaurus (Sco OB2), Handbook of Star Forming Regions, Vol. II. Astron. Soc. Pac., San Francisco, p. 235
Preibisch T., Zinnecker H., 1999, AJ, 117, 2381
Preibisch T., Guenther E., Zinnecker H., Sterzik M., Frink S., Roeser S., 1998, A&A, 333, 619
Preibisch T., Guenther E., Zinnecker H., 2001, AJ, 121, 1040
Preibisch T., Brown A. G. A., Bridges T., Guenther E., Zinnecker H., 2002, AJ, 124, 404
Raghavan D. et al., 2010, ApJS, 190, 1
Randich S., Schmitt J. H. M. M., Prosser C. F., Stauffer J. R., 1995, A&A, 300, 134
Randich S., Aharpour N., Pallavicini R., Prosser C. F., Stauffer J. R., 1997, A&A, 323, 86
Reid N., 2003, MNRAS, 342, 837
Riaud P., Mawet D., Absil O., Boccaletti A., Baudoz P., Herwats E., Surdej J., 2006, A&A, 458, 317
Riaz B., Gizis J. E., Harvin J., 2006, AJ, 132, 866
Ribas Á., Bouy H., Merín B., 2015, A&A, 576, A52
Rizzuto A. C., Ireland M. J., Robertson J. G., 2011, MNRAS, 416, 3108
Rizzuto A. C., Ireland M. J., Kraus A. L., 2015, MNRAS, 448, 2737
Rodriguez D. R., Bessell M. S., Zuckerman B., Kastner J. H., 2011, ApJ, 727, 62
Röser S., Schilbach E., Schwan H., Kharchenko N. V., Piskunov A. E., Scholz R.-D., 2008, A&A, 488, 401
Satyvaldiev V., 1972, Astron. Tsirkulyar, 728, 5
Satyvoldiev V., 1982, Perem. Zvezdy Prilozhenie, 4, 109
Schlieder J. E., Lépine S., Rice E., Simon M., Fielding D., Tomasino R., 2012, AJ, 143, 114
Schwartz R. D., 1977, ApJS, 35, 161
Sciortino S., Damiani F., Favata F., Micela G., 1998, A&A, 332, 825
Shobbrook R. R., 1983, MNRAS, 205, 1215
Skrutskie M. F. et al., 2006, AJ, 131, 1163
Slesnick C. L., Carpenter J. M., Hillenbrand L. A., 2006, AJ, 131, 3016
Slesnick C. L., Hillenbrand L. A., Carpenter J. M., 2008, ApJ, 688, 377
Soderblom D. R., Jones B. F., Balachandran S., Stauffer J. R., Duncan D. K., Fedele S. B., Hudon J. D., 1993, AJ, 106, 1059
Soderblom D. R., Hillenbrand L. A., Jeffries R. D., Mamajek E. E., Naylor T., 2014, in Beuther H., Klessen R. S., Dullemond C. P., Henning T., eds, Protostars and Planets VI. Univ. Arizona Press, Tucson, p. 219
Somers G., Pinsonneault M. H., 2015, ApJ, 807, 174
Song I., Zuckerman B., Bessell M. S., 2003, ApJ, 599, 342
Song I., Zuckerman B., Bessell M. S., 2012, AJ, 144, 8
Spinrad H., 1962, ApJ, 135, 715
Stauffer J. R., Schultz G., Kirkpatrick J. D., 1998, ApJ, 499, L199
Stauffer J. R., Jones B. F., Backman D., Hartmann L. W., Barrado y Navascués D., Pinsonneault M. H., Terndrup D. M., Muench A. A., 2003, AJ, 126, 833
Stephenson C. B., 1986, ApJ, 300, 779
Stocke J. T., Morris S. L., Gioia I. M., Maccacaro T., Schild R., Wolter A., Fleming T. A., Henry J. P., 1991, ApJS, 76, 813
Strom S. E., 1994, in Caillault J.-P., ed., ASP Conf. Ser. Vol. 64, Cool Stars, Stellar Systems, and the Sun. Astron. Soc. Pac., San Francisco, p. 211
Struve O., Rudkjøbing M., 1949, ApJ, 109, 92
Thackeray A. D., 1966, Mem. RAS, 70, 33
The P.-S., 1962, Contrib. Bosscha Obs., 15, 0
The P.-S., 1964, PASP, 76, 293
Tognelli E., Prada Moroni P. G., Degl'Innocenti S., 2011, A&A, 533, A109
Torres G., Ribas I., 2002, ApJ, 567, 1140
Torres C. A. O., Quast G. R., da Silva L., de La Reza R., Melo C. H. F., Sterzik M., 2006, A&A, 460, 695
Torres C. A. O., Quast G. R., Melo C. H. F., Sterzik M. F., 2008, Reipurth B. ed., Young Nearby Loose Associations. Handbook of Star Forming Regions, Vol. II. Astron. Soc. Pac., San Francisco, p. 757

van Leeuwen F., 2007, A&A, 474, 653
Vazquez R. A., Feinstein A., 1991, A&AS, 87, 383
Viana Almeida P., Santos N. C., Melo C., Ammler-von Eiff M., Torres C. A. O., Quast G. R., Gameiro J. F., Sterzik M., 2009, A&A, 501, 965
Voges W. et al., 1999, A&A, 349, 389
Voges W. et al., 2000, IAU Circ., 7432, 3
Walter F. M., Vrba F. J., Mathieu R. D., Brown A., Myers P. C., 1994, AJ, 107, 692
Webb R. A., 2000, PhD thesis, University of California
Weinberger A. J., Anglada-Escudé G., Boss A. P., 2013, ApJ, 762, 118
White R. J., Gabor J. M., Hillenbrand L. A., 2007, AJ, 133, 2524
Wichmann R., Sterzik M., Krautter J., Metanomski A., Voges W., 1997, A&A, 326, 211
Wichmann R., Covino E., Alcalá J. M., Krautter J., Allain S., Hauschildt P. H., 1999, MNRAS, 307, 909
Wright E. L. et al., 2010, AJ, 140, 1868
Wright N. J., Parker R. J., Goodwin S. P., Drake J. J., 2014, MNRAS, 438, 639
Wright N. J., Bouy H., Drew J. E., Sarro L. M., Bertin E., Cuillandre J.-C., Barrado D., 2016, preprint (arXiv:1605.03583)
Yee J. C., Jensen E. L. N., 2010, ApJ, 711, 303
Zacharias N., Finch C. T., Girard T. M., Henden A., Bartlett J. L., Monet D. G., Zacharias M. I., 2013, AJ, 145, 44
Zhang K., Pontoppidan K. M., Salyk C., Blake G. A., 2013, ApJ, 766, 82
Zuckerman B., Song I., 2004, ARA&A, 42, 685
Zuckerman B., Webb R. A., Schwartz M., Becklin E. E., 2001, ApJ, 549, L233

SUPPORTING INFORMATION

Additional Supporting Information may be found in the online version of this article:

Table 1. Photometry and proper motion data for candidates in the Sco–Cen region.
Table 3. Infrared photometry and infrared excesses for Members of Sco–Cen.
Table 4. Membership properties for Sco–Cen candidates.
Table 7. Stellar properties for Sco–Cen members.
Table 8. Objects rejected as Sco–Cen members.
Table 9. Stellar parameters for Sco–Cen G-type stars
(http://www.mnras.oxfordjournals.org/lookup/suppl/doi:10.1093/mnras/stw1300/-/DC1).

Please note: Oxford University Press is not responsible for the content or functionality of any supporting materials supplied by the authors. Any queries (other than missing material) should be directed to the corresponding author for the article.

This paper has been typeset from a TEX/LATEX file prepared by the author.